INVITED PAPER

Waveform Design and Signal Processing Aspects for Fusion of Wireless Communications and Radar Sensing

The authors of this paper argue that combining radar and communication systems can allow both environmental sensing and V2X communications to be performed more efficiently.

By Christian Sturm, *Student Member IEEE*, and Werner Wiesbeck, *Fellow IEEE*

ABSTRACT | Since traditional radar signals are "unintelligent," regarding the amount of information they convey on the bandwidth they occupy, a joint radar and wireless communication system would constitute a unique platform for future intelligent transportation networks effecting the essential tasks of environmental sensing and the allocation of ad-hoc communication links, in terms of both spectrum efficiency and cost-effectiveness. In this paper, approaches to the design of intelligent waveforms, that are suitable for simultaneously performing both data transmission and radar sensing, are proposed. The approach is based on classical phase-coded waveforms utilized in wireless communications. In particular, requirements that allow for employing such signals for radar measurements with high dynamic range are investigated. Also, a variety of possible radar processing algorithms are discussed. Moreover, the applicability of multiple antenna techniques for direction-of-arrival estimation is considered. In addition to theoretical considerations, the paper presents system simulations and measurement results of complete "RadCom" systems, demonstrating the practical feasibility of integrated communications and radar applications.

KEYWORDS | ACC; digital beam-forming; MIMO; OFDM; radar; RadCom; SRR; V2I; V2V

Manuscript received June 18, 2010; revised October 10, 2010, March 5, 2011, and March 15, 2011; accepted March 15, 2011. Date of publication May 27, 2011; date of current version June 17, 2011.

The authors are with the Institut für Hochfrequenztechnik und Elektronik, Karlsruhe Institute of Technology, 76131 Karlsruhe, Germany (e-mail: christian.sturm@kit.edu; werner.wiesbeck@kit.edu).

Digital Object Identifier: 10.1109/JPROC.2011.2131110

I. INTRODUCTION

In current technological development, radio frequency front-end architectures in radar and wireless communication technologies have become more and more similar. In particular, an increasing number of functions, traditionally realized by hardware components, are being replaced by digital signal processing. At the same time, the carrier frequencies used for communication systems, have shifted to the microwave regime and have become of the same order of magnitude as those traditionally used for radar applications. Hence, a joint radio-frequency hardware platform for communications and radar applications could easily be realized with today's technology. Such a kind of platform would offer unique possibilities for novel system concepts and applications.

Even more important, by using a joint waveform for both applications, the occupied spectrum would be used very efficiently and both applications could be operated simultaneously, which would guarantee a permanent availability of both functions, and help to partially overcome the limited availability of spectral resources. Such systems, providing radar and communication functions on a single hardware platform with a single waveform, will be denoted in the following with the acronym "RadCom."

There is a large area of applications which would possibly benefit from the availability of RadCom systems, in particular, intelligent transportation applications requiring both communication links to other vehicles and active environment sensing functions. With a suitable system platform, all vehicles on the road could interact in a

cooperative radar sensor network, providing unique safety features and intelligent traffic routing.

Moreover, the market introduction of a system jointly offering communication and radar functions, would be much easier, compared to one just offering pure car-to-car communication features. Since a car-to-car communication system could only provide information when communication partners are present, at the time of market introduction there would not be much incentive for possible customers to have their cars equipped with a pure car-to-car communication system. A RadCom system, however, would always provide a benefit to the customer, independently from the level of market penetration, due to its radar sensing functionality.

Furthermore, it could be expected that in a joint system both applications would profit from sharing information with one another. For example, the radar application could use the information distributed on the communication network in order to increase its detection probability and precision. Finally, even a complete fusion of the radar images acquired from different platforms would be possible, which would allow an extension of the sensor range far beyond the propagation limits.

The main challenge in RadCom development lies in finding suitable waveforms that can be simultaneously employed for information transmission and radar sensing. Therefore, the main scope of this paper is identifying and evaluating different approaches for that purpose. It should be emphasized, that, even if the investigations presented in this paper focus on automotive applications, the discussed concepts and waveforms can be employed in any application scenario that requires radar sensing and communication at the same time, e.g., aeronautical and military applications.

Classical radar waveform design aims at creating waveforms with optimum autocorrelation properties, which guarantees the high dynamic range of the measurements when applying correlation processing in the receiver. The most popular example fulfilling this requirement are linear frequency modulated (LFM) pulses, also known as "chirp" signals [1]. The most intuitive approach for designing a joint waveform, hence, would be to use the linear frequency modulation also for encoding data, as e.g., done in [2]. A more sophisticated approach for covert communication with LFM pulses has been reported in [3]. Both approaches, however, share the disadvantage that the communication symbol rate corresponds to the chirp rate only, which is typically orders of magnitude lower than the symbol rate that is achieved by a dedicated communication system in the same bandwidth. Therefore, from the communications perspective, this approach is not optimal and will not be considered in the following.

In order to achieve better communications performance in terms of symbol rates, continuous transmit signals, originating from digital communications, have to be applied. A typical communication waveform with good autocorrelation properties is the spread spectrum signal, which is a well-known candidate for joint radar and communications applications [4]. In addition, advanced concepts, based on multicarrier communication waveforms, have appeared recently [5]. With multicarrier waveforms, processing techniques in the frequency domain can be applied that allow relaxing the autocorrelation requirement. The main sections of this paper explicitly deal with continuous single-carrier and multicarrier waveforms, since these concepts are the most promising ones regarding their ability for providing high-performance in both radar and communications.

Not only the employed waveform, but also general system parameters, e.g., the bandwidth, have to be chosen according to the requirements derived from both applications. At first glance, the conditions for optimum signal parameters, from the communications and radar perspective, seem different. That is, in order to achieve high resolution, a radar sensor needs a large signal bandwidth, which is usually much wider than the bandwidth of typical communication signals. The discussion on waveform design includes detailed considerations regarding a suitable choice of the system parameters, leading to an optimum solution for both applications. Furthermore, the waveform design should satisfy a number of additional requirements, most importantly, it should be possible to perform radar sensing with arbitrary transmit data. Only in that case is an efficient reuse of the spectrum possible.

While the Doppler shift of the received signal, which occurs in environments with moving objects, represents a deteriorating factor for the quality of information transmission, it contains valuable information on the velocities of the reflecting objects at the same time. Hence a strategy must be found that allows for tolerating the Doppler shift in the case of information transmission and for exploiting the velocity information in the radar processing. The radar processing algorithm should support the independent estimation of range and velocity of multiple objects. The acquisition of Doppler information, in addition to a simple range measurement, is, in particular, important for active vehicular safety applications, i.e., pre-crash detection.

In practical automotive applications, in addition to the range and the velocity also the azimuth position of objects must be determined, in order to get the full 2D scenario information. However, rotating narrow-beam antennas, as typically utilized for surveillance radar systems, are hardly applicable in automotive radar and would also imply low update rates and restricted communication coverage. A practical solution is to use digital beam-forming (DBF) techniques, which is currently an important research area. In this approach, the received signals from multiple antenna elements, with a wider, dedicated coverage, are first individually converted to base-band and digitized. Then, they are processed to form an arbitrary, but limited, number of beams covering the illuminated scene [6]. It can be foreseen that this technique will provide advanced

flexibility and performance in many radar applications, from small automotive radar sensors (adaptive cruise control, short range parking aid and so on) to space-borne synthetic aperture radars [7]. Because of the significant processing advantages, compared to classical concepts, digital beam-forming allows one to cover a wide area while simultaneously focusing on any spot in this area. Also, for communications applications, multiple antenna techniques have gained significant interest, to the extent that commercial systems are already available. These techniques are usually denoted MIMO (multiple-input–multiple-output) or Smart Antennas. The general idea is to combine the signals received from multiple antennas in an intelligent way in order to achieve the best signal-to-noise ratio and highest data rate. The signal combination is performed in the digital domain, after conversion to baseband, which offers the opportunity of applying a variety of algorithms. This procedure can also be interpreted as adaptive processing of virtual beam patterns for enhanced directivity gain and interference suppression. An examination of both concepts, namely, MIMO and DBF, makes their similarities immediately evident. In particular, both are based on a structure of distributed antennas, both use the same receiver concept with baseband conversion and sampling of signals from individual antennas, both apply fully digital signal processing, and both have the same idea of maximizing the information by creating virtual array beam patterns. Regarding these considerations, DBF radar and MIMO communications could ideally be integrated into RadCom systems to achieve spatial resolution and performance improvement.

For the joint implementation of DBF radar and MIMO communications, a suitable operation frequency band has to be found. Wireless network standards like WLAN typically operate in ISM bands, which can be used from any device without requiring a license. The radar application requires a certain minimum bandwidth, on the order of at least 100 MHz, for sufficient resolution. The 24 GHz ISM band is the lowest worldwide available ISM band that fulfils this requirement. There already exist highly integrated commercial radar sensors operating in this band for automotive applications [8]. However, the achievable range for communications decreases drastically with increasing carrier frequency, due to the increasing free space attenuation and the decreasing influence of diffraction. Keeping in mind the minimum bandwidth requirement, the 24 GHz ISM band currently seems the best choice for a RadCom system that can be operated license-free.

In the following sections, detailed considerations regarding the possibilities and remaining constraints for a complete integration of wireless communications and radar sensing will be presented, with a special focus on intelligent transportation applications. In particular, possible approaches to waveform design, as well as suitable processing techniques for range, Doppler and direction of arrival estimation from the reflected signal, will be discussed in detail and verified by system simulations and measurements. In Section II, waveforms that can be applied in both, wireless communications and radar, will be identified and described; a typical RadCom application scenario and detailed requirements will be discussed. In Section III, an approach for applying single-carrier signals in combination with spread spectrum techniques will be discussed and evaluated with simulations. Similarly, Section IV presents an advanced approach, based on multicarrier waveforms. For the multicarrier approach, both simulation and measurement results will be presented. In Section V, the application of multiple antenna processing techniques will be discussed. Finally, in Sections VI and VII, considerations regarding the range of operation of a practical system implementation in the 24 GHz band will be presented, and general conclusions will be drawn.

II. WAVEFORM DESIGN CONSIDERATIONS AND REQUIREMENTS

The first step toward the implementation of RadCom systems is to identify waveforms that are suitable for both wireless communications and radar applications. The selection of the waveforms has to be based on the requirements for the radar, in particular, pertaining to the determination of object range, Doppler and angular offset. For all three, dynamic range and resolution are critical requirements for object detection and separation. In addition, in dense traffic, the waveform should be robust against interference and noise.

For communications, the data rate and the bit error rate are the most stringent parameters. As for the radar function, the waveform should be robust against interference, noise, and distortion due to multipath-propagation. In order to provide high performance in terms of bit rate, a continuous signal, with a sufficiently high symbol rate, has to be chosen. There is no demand to hide or protect the information content, since the transmitted information is intended to reach all RadCom systems in the neighborhood.

Presently, for automotive radar applications, waveforms such as FM-CW (frequency modulated continuous wave), and to a lesser extent pulsed-FM, are primarily applied. For other radar applications, numerous other waveforms are known (chirp, pseudorandom, staggered, phase and frequency coding etc.) [1]. For digital communications, especially mobile communications, two concepts dominate waveform design and application, namely, single-carrier waveforms, on the one hand, and multicarrier waveforms, also often denoted Orthogonal Frequency Division Multiplexing (OFDM), on the other. Most recent digital communications standards apply discrete phase modulation techniques in terms of phase shift keying (BPSK, QPSK, 8 PSK) or quadrature amplitude modulation schemes of higher order (16 QAM, 64 QAM). In propagation scenarios, with multipath propagation, Doppler and fading, only low-order modulation schemes, like BPSK and

QPSK, can be successfully implemented. This condition holds at least in a broadcast scenario with multiple receivers and individual propagation channels, in which adaptive modulation cannot be applied. Additional robustness can be achieved by applying spread spectrum techniques (e.g., direct sequence spread spectrum, DSSS). OFDM waveforms incorporate frequency diversity, which, through appropriate coding, can be exploited for increasing the robustness of the transmission. These techniques offer a number of advantages, such as the availability of processing gain at the receiver, a whitening of the signal spectrum, and a reduction of the power spectral density.

For radar applications, there also exist principles similar to DSSS that are based on discrete phase modulation and binary pseudorandom sequences. A typical example are m-sequence radars, which employ pseudorandom m-sequences for discrete phase modulation, in order to create a noise-like transmit signal with good autocorrelation properties [9]. The applicability of multicarrier waveforms for radar purposes has been demonstrated as well [10]. Furthermore, also in radar applications a processing gain is available from DSSS or OFDM waveforms, which makes the system robust and allows for operation in scenarios with low-received signal power or high-interference levels.

Thus, waveforms with discrete phase modulation offer a joint basis for radar and communications, fulfilling the requirements for both applications.

Quadrature amplitude modulated single-carrier waveforms (including the special case of phase-coded signals) are generally represented by the following expression for the complex baseband signal:

$$x(t) = \sum_{i=0}^{N_{\mathrm{sym}}-1} a(i)g(t - iT) \tag{1}$$

with N_{sym} being the number of modulation symbols composing the signal frame, T denoting the symbol duration, $g(t)$ being the elementary baseband pulse shape, and $a(i)$ representing the discrete amplitude and phase states obtained through any PSK or QAM modulation scheme.

An OFDM multicarrier signal can be regarded as a parallel stream of multiple single-carrier signals with orthogonal carrier waveforms, each modulated with different transmit data. Analytically the signal can be expressed as:

$$x(t) = \sum_{\mu=0}^{N_{\mathrm{sym}}-1} \sum_{n=0}^{N_c-1} a(\mu N_c + n) \exp(j2\pi f_n t) \mathrm{rect}\left(\frac{t - \mu T_{\mathrm{OFDM}}}{T_{\mathrm{OFDM}}}\right) \tag{2}$$

with μ representing the individual OFDM symbol index within the total amount of N_{sym} OFDM symbols, n denoting the individual subcarrier index from a total amount of N_c subcarriers, a being the complex modulation symbols, f_n being the individual subcarrier frequency, $T_{\mathrm{OFDM}} = T + T_G$ being the total OFDM symbol duration composed of an elementary symbol duration T and a guard interval duration T_G, and $\mathrm{rect}(t/T_{\mathrm{OFDM}})$ describing a rectangular window of duration T_{OFDM}. In contrast to single-carrier waveforms, for OFDM transmission generally a rectangular pulse shape is applied for the individual subcarriers. The occupation of the spectrum, over time, by the different subcarriers and OFDM symbols, is illustrated in Fig. 1. With a high number of sub-carriers, a quasi-constant power spectral density, over time and frequency, is achieved, and the output signal appears noise-like.

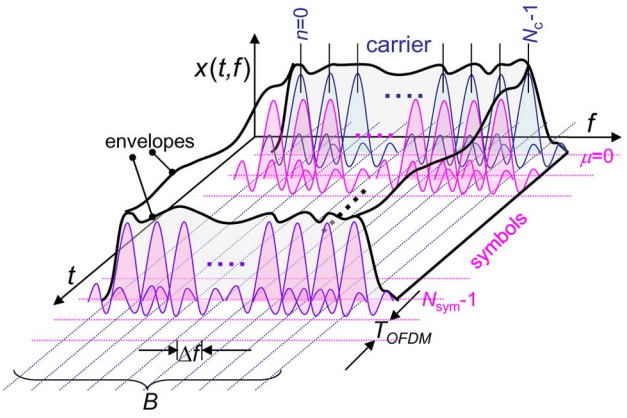

Fig. 1. *Time and frequency structure of an OFDM signal.*

In order for the individual subcarriers to become orthogonal, and not interfere, the following condition must hold:

$$f_n = n\Delta f = \frac{n}{T}, \quad n = 0, \ldots, N_c - 1 \tag{3}$$

i.e., the separation, Δf, between the subcarriers, directly results in the inverse of the elementary OFDM symbol duration T. Compared to the symbol duration of a single-carrier transmission, with the same data rate, the elementary OFDM symbol duration is increased by the factor N_c, which makes the signal robust against fast fading effects. The *guard interval* or *cyclic prefix*, which is a partial cyclic repetition of the time domain signal of the duration T_G corresponding to the maximum expected multipath delay, allows for fully compensating multipath propagation effects. The cyclic prefix is typically prepended at the beginning of the OFDM symbol, occupying the interval $[0, T_G)$ within the total OFDM symbol duration T_{OFDM}. The receiver only evaluates the interval $[T_G, T_{\mathrm{OFDM}})$, which contains no inter-symbol interference caused by multipath propagation [11].

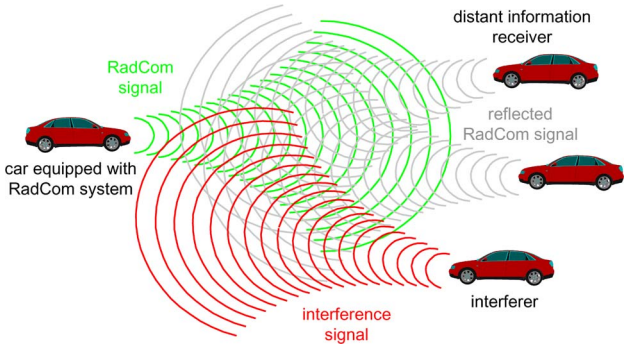

Fig. 2. ***RadCom application scenario.***

The general principle for the operation of a RadCom system is to transmit arbitrary user data with one of the waveforms described in (1) and (2), if necessary including a suitable channel coding strategy. The considered application scenario is illustrated in Fig. 2. The RadCom signal (colored in green) is transmitted from the car on the left. This signal transports information to distant receivers. At the same time, this RadCom signal is reflected from objects, including cars, in the neighborhood (reflected signal depicted in gray). The RadCom system observes the echoes of its own transmit signal, and detects the presence of reflecting objects, and their distance and relative velocity, by applying suitable processing algorithms. This task can be interpreted as a detection of point targets. Imaging of the reflecting objects themselves is typically not considered, and would not be possible with a bandwidth on the order of 100 MHz. The evaluation of the reflected transmit signal is performed by digital signal processing, hence arbitrary algorithms can be applied, either operating in time domain or frequency domain. For radar processing, it can be assumed that the transmitted signal is perfectly known at the radar receiver. As it is intended to use continuous transmit signals, the transmit signal duration will be much longer than the roundtrip propagation time of the signal. This implies that the receiver must be able to listen during transmission, which requires proper decoupling of the transmit and the receive antenna. Also, it has to be assumed that there are several systems operating in parallel, in the same band, and interference from other RadCom platforms will occur (red interference signal).

In the following sections it is, in particular, addressed, how suitable radar processing algorithms can be implemented for both types of waveforms, and which requirements regarding the properties of the transmit signal must be respected. Moreover, the radar sensing performance that can be achieved with the different waveforms is investigated in detail; the main criterion is the dynamic range that can be achieved. In this context, in the following it is distinguished between the dynamic range of the radar image, which describes the ratio between the main peak in the image and the average noise floor, and the peak-to-side-lobe ratio (PSL), which describes the ratio between the main peak and the maximum side-lobe value, either caused by Fourier side-lobes or imperfect autocorrelation properties.

III. THE SPREAD SPECTRUM SINGLE-CARRIER APPROACH

A. Signal Coding

In this section a RadCom implementation, based on single-carrier signals is discussed. Single-carrier signals do not incorporate frequency diversity, hence the natural approach, in order to make them suitable for radar measurements, is to optimize their autocorrelation properties and perform time-domain correlation processing in the receiver. As it has already been discussed in Section II, coding of the transmit signal with pseudorandom sequences is applied in the case of spread spectrum communications, as well as, in the case of m-sequence radar. Using a pure m-sequence, with the elements mapping a 2-PSK alphabet $a(i) \in \{1, -1\}$ for modulating the single carrier waveform according to (1), a transmit signal with quasi-optimum autocorrelation properties results [9]. First considerations regarding the implementation of joint radar and communications applications, based on spread spectrum signals, have already been reported many years ago [4], [12]. The basic idea is to apply spread spectrum coding with a sufficiently high spreading factor, so that the resulting signal inherits the good autocorrelation properties of the spreading code, which is a pseudorandom binary code, e.g., an m-sequence. In the following, a standard spread spectrum transmission, as typically applied in digital communications, is considered, in which each element $a(i)$ of the data sequence is replaced by the result of its multiplication with L elements of a code sequence [13]. L is denoted spreading factor and the length of the resulting symbol sequence $c(i)$ amounts LN_{sym}. A more detailed description of the encoding procedure can be found in [14]. The introduction of redundancy with the spread spectrum coding reduces the user data rate in proportion to the spreading factor, provided that the symbol rate after the encoder is kept constant. On the other hand, spread spectrum coding can be exploited for user separation by code division multiple access (CDMA). Hence, this approach provides an inherent support for multiuser operation with standard CDMA techniques.

In the following, the correlation processing for performing the radar measurement with the reflected signal is addressed in detail. If the transmitted signal is scattered back from an object located in the range R, the received signal $y(t)$ can be expressed as

$$y(t) = Ax\left(t - \frac{2R}{c_0}\right) = A\sum_{i=0}^{LN_{\mathrm{sym}}-1} c(i)\, g\left(t - \frac{2R}{c_0} - iT\right) \quad (4)$$

with the complex amplitude factor A describing the attenuation and phase shift occurring due to the propagation and scattering process, and c_0 being the speed of light. The radar processor estimates the range to the scattering object by calculating the cross-correlation function, $r_{yx}(t,\tau)$, between the received and the transmitted signal

$$r_{yx}(t,\tau)=\int_{t=0}^{LN_{\text{sym}}T}\left(A\sum_{i=0}^{LN_{\text{sym}}-1}c(i)g\left(t-\frac{2R}{c_0}-iT\right)\right)\times\left(\sum_{k=0}^{LN_{\text{sym}}-1}c(k)g(t-\tau-kT)\right)dt \quad (5)$$

which can be rewritten as

$$r_{yx}(t,\tau)=A\sum_{i=0}^{LN_{\text{sym}}-1}\sum_{k=0}^{LN_{\text{sym}}-1}c(i)c(k)\int_{t=0}^{LN_{\text{sym}}T}g\left(t-\frac{2R}{c_0}-iT\right)\times g(t-\tau-kT)\,dt. \quad (6)$$

Obviously, the integral in (6), describes the autocorrelation function $r_{gg}(\tau)$ of the baseband pulse shape $g(t)$ shifted in time

$$r_{yx}(\tau)=A\sum_{i=0}^{LN_{\text{sym}}-1}\sum_{k=0}^{LN_{\text{sym}}-1}c(i)c(k)r_{gg}\left(\tau-\frac{2R}{c_0}+(k-i)T\right). \quad (7)$$

Hence, both the properties of the code sequence and the shape of the autocorrelation function of the baseband pulse have a direct impact on the result of the correlation performed in the receiver. However, a simplification of (7) is practically impossible, due to the discrete nature of k and i, and the continuous nature of τ. If it is assumed, that $g(t)$ is the impulse response of a root raised cosine roll-off filter with its maximum peak at $t=0$, then $r_{gg}(\tau)$ will show a peak value under the condition $\tau=0$. In order that the time shifted autocorrelation function in (7) contributes its maximum value, the following condition must hold:

$$\tau=\frac{2R}{c_0}-(k-i)T. \quad (8)$$

However, for a peak to appear in $r_{yx}(\tau)$ also the sequences $c(i)$ and $c(k)$ must be shifted in a way that they superimpose coherently. This is the case for $\tau=0$ resulting in

$$k=i+\left\lfloor\frac{2R}{c_0T}\right\rfloor. \quad (9)$$

Hence, for an index shift determined by the distance of the object a main peak appears in $r_{yx}(\tau)$. For other combinations of k and i, $r_{gg}(\tau)$ contributes reduced values with a height determined by the side-lobe levels of $g(t)$. Moreover, also the imperfect crosscorrelation properties of the transmit symbol sequence $c(i)$ contribute additional side-lobes. Both effects interact and result in complex side-lobe shapes. For optimum performance, a pulse shape $g(t)$ with low side-lobe levels should be applied. The maximum peak-to-side-lobe ratio that can be achieved has to be determined by numerical simulations. The result in (7) also indicates that a processing gain, corresponding to the frame length LN_{sym}, is achieved. Since the performed correlation is a linear operation, an arbitrary number of scatterers, at different distances, can be resolved and will appear as different peaks in the radar image.

B. Code Sequences and System Performance

There are different requirements concerning the properties of the applied pseudorandom sequence. For the communications application, it is necessary to have a certain number of orthogonal sequences available, which can be assigned to the different users. If it is supposed that the different users are not synchronized in time, this requirement becomes even stronger. In this case, the sequences would have to possess ideal cross-correlation properties, i.e., the sequences would have to be orthogonal for any time shift. For the operability of the radar processing, the employed transmit sequences must possess ideal autocorrelation properties, i.e., their autocorrelation function must result in one single peak. If both functions are to be performed simultaneously, the pseudorandom sequence must fulfill both requirements, i.e., possess ideal cross-correlation and ideal autocorrelation properties. It has been analytically proven that both conditions cannot be simultaneously fulfilled; there is a joint lower bound on the maximum of the cross-correlation function and the maximum side-lobe of the autocorrelation function (Welch bound) [15]. The minimum side-lobe level that can be achieved in the case of periodic correlation is

$$\max\{|r_{cc}(i\neq 0)|,|r_{c_1c_2}(i)|\}\geq\sqrt{\frac{L^2(M-1)}{LM-1}} \quad (10)$$

with L denoting the length of the pseudorandom sequence and M being the number of different code sequences that

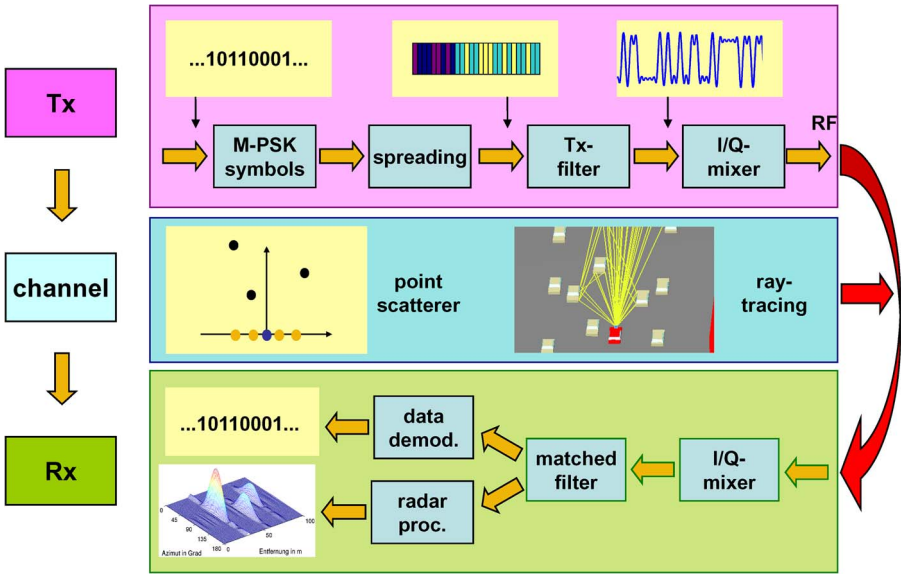

Fig. 3. *Spread spectrum radar system and scenario simulation tool.*

can be derived from the generation law. The maximum of the autocorrelation function increases linearly with the code length L, whereas, according to (10), the side-lobes are increasing approximately with the square root of L. Thus, with a sufficiently high code sequence length and the choice of a proper code family, very low side-lobe levels can be achieved. Well-known code families with a small amount of members M are the so-called *preferred* m-sequences (a subset of all possible m-sequences of a certain order) [16] and *Kasami* sequences [17]. Other popular pseudorandom codes that will be considered in the following investigations are Gold sequences [18] and chaotic sequences [19], which are, in particular, interesting for security applications due to their unpredictable behavior.

C. System Simulation Model

In order to demonstrate the operability of the proposed concept, and to investigate the system performance pertaining to the achievable radar peak-to-side-lobe ratio, a complete system model has been implemented in MatLab. The system model is shown in the Fig. 3.

In the transmitter, spread spectrum coding is applied to a randomly generated user data sequence, then each encoded transmit symbol $c(i)$ is mapped onto the elementary baseband pulse in order to create a continuous baseband signal according to (1). The resulting baseband signal is converted to a carrier frequency in the I/Q mixer. In the propagation simulation, the signal propagation and the scattering from an arbitrary number of point scatterers is modeled. For each scatterer, the time delay, attenuation, and phase shift are individually calculated. Then, the scattered signals are superimposed. Alternatively, a propagation simulator, for realistic road scenarios, based on ray-tracing, can be employed. Finally, in the receiver, the radar processing is performed. In Table 1, a summary of the most important system parameters of the simulation model is provided.

Table 1 System Parameters of the Spread Spectrum Simulation Model

Parameter	Value
Modulation	BPSK
Spreading factor L	variable (15,31,63,127,255)
Symbol rate (at encoder output)	48 MSymbols/s
Transmit filter	Root raised cosine roll-off (r=1)
Transmit signal bandwidth	≈ 96 MHz
Range resolution	≈ 2.5 m
Transmit frame length N_{sym}	256 user data symbols

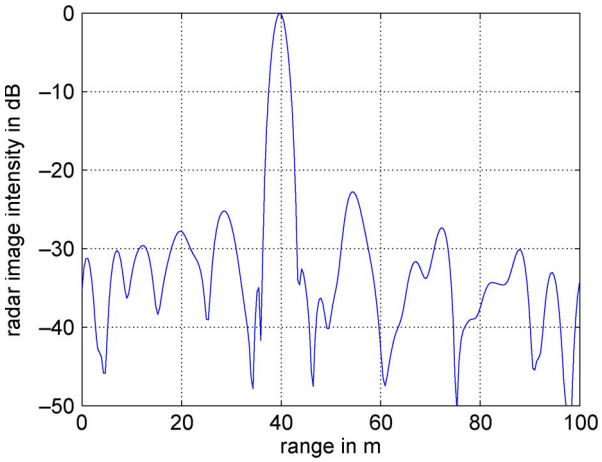

Fig. 4. *Calculated radar range profile with m-sequence and $L = 15$.*

The symbol rate referring to the encoded symbols $c(i)$ is kept at a constant value at the encoder output, in order to have a constant signal bandwidth independent from the applied spreading factor. With these parameters, an m-sequence as pseudorandom code, and a spreading factor of $L = 15$, the radar processing of one point scatterer at a distance of $R = 40$ m has been simulated. The integration time of the radar processing corresponds to one transmit frame length of $N_{\mathrm{sym}} = 256$ user data symbols, or $N_{\mathrm{sym}}L = 3480$ code symbols, respectively, corresponding to a frame duration of 36.6 μs. The resulting radar range profile is shown in Fig. 4.

In the calculated radar range profile, the point scatterer can be clearly identified. The 3 dB-width of the scatterer in the image amounts to, approximately, 2.5 m, which is larger than the ideally achievable 1.5 m. The widening is caused by the root raised cosine roll-off filter, which can be interpreted as a $\cos^2$-window in the spectral domain. The side-lobes, caused by the interaction of the side-lobes of the baseband pulse shape and the side-lobes resulting from the nonideal autocorrelation properties of the transmit sequence, are clearly visible and look different from typical Fourier transform side-lobes. Nevertheless, already with a relatively low spreading factor of $L = 15$, a relative maximum side-lobe level of -23 dB is achieved.

In addition to the spreading factor, the total length of the pseudorandom code sequence and the sequence type have a strong impact on the side-lobe performance. Different types of pseudorandom sequences have been implemented for the spread spectrum encoding. Moreover, two approaches of spread-spectrum encoding have been distinguished and tested. In the case of *short code* encoding, the pseudorandom sequence repeats with every user data symbol, i.e., the sequence length is equal to the spreading factor. In the case of *long code* encoding, the pseudorandom sequence is much longer than the spreading factor and will not even repeat within one transmit frame. Also, interference from a second system has been included in the simulations. An interfering signal from a second system was calculated with the same transmitter model, but using a different pseudorandom sequence of the same type for the encoding procedure. In a first step, a fixed signal-to-interference ratio of 0 dB has been assumed. Fig. 5 shows an overview of the peak-to-side-lobe ratio (PSL) that can be achieved in the addressed system concept with different code types and different encoding principles, as a function of the spreading factor. All values have been obtained from simulations investigating the maximum side-lobe levels when simulating the presence of one point scatterer.

The following observations are obvious, from an examination of Fig. 5. Using long-code encoding, a drastically higher PSL can be achieved compared to using short-code encoding. With long-code encoding both, m-sequences and Kasami sequences, which are typical representatives of code sequence families with few different members, perform similarly and well. With a spreading factor of $L = 512$, a dynamic range of 40 dB and more can be achieved, even in the presence of interference. Similarly, chaotic sequences perform comparably well. With short-code encoding, performance clearly degrades. In particular, for low spreading factors the PSL decreases by more than 10 dB, compared to long-code encoding. The worst result is obtained with Gold sequences, which are optimized for orthogonality and are known to possess rather poor autocorrelation properties.

In order to investigate the performance in the presence of interference more deeply, simulations are performed with varying interference level. In these simulations, only short-code encoding with m-sequences is considered. The

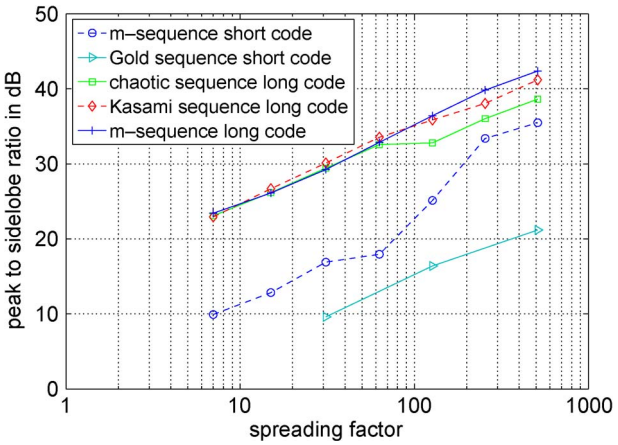

Fig. 5. *Achievable peak-to-side-lobe ratio with different types of pseudorandom spreading sequences.*

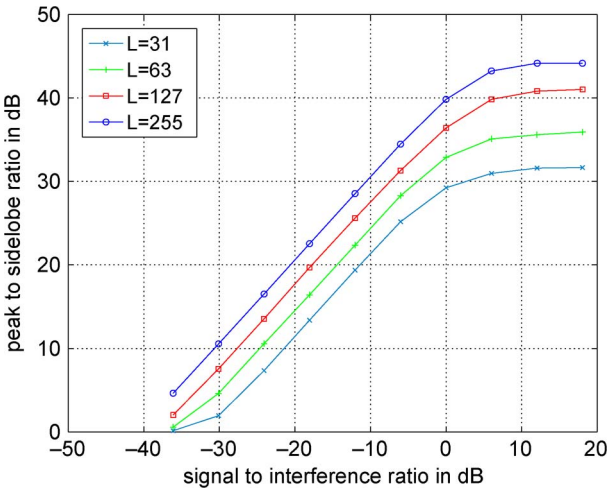

Fig. 6. *Achievable peak-to-side-lobe ratio in the presence of interference from a second system for different spreading factors.*

peak-to-side-lobe ratio that is available dependent on the signal-to-interference ratio (SIR) measured at the input of the radar processor, is plotted in Fig. 6 for different spreading factors.

For a signal-to-interference ratio below 0 dB, the available dynamic range decreases almost linearly with increasing interference power. Starting approximately at a signal-to-interference ratio of 10 dB, there appears a saturation of the dynamic range and the performance does not improve distinctly for better signal-to-interference ratios. This results from the fact that, in this area, the performance is only limited by the properties of the code sequence and not by the interfering signal.

It should be mentioned that similar investigations have also been conducted with an additive white noise signal, instead of interference. The dynamic range turned out to be identical, compared to the results that have been obtained in the case of interference. This coincidence is, obviously, a result of the noise-like properties of the spread spectrum signal. Finally, it can be concluded that the studied waveform design concept offers a peak-to-side-lobe ratio on the order of 30 to 40 dB for radar applications, which degrades in the presence of very strong interference. Through a flexible choice of the spreading factor, the system configuration can be adapted to different environmental constraints.

D. Influence of Doppler Shift

For applications in vehicular environments, it must be expected that the received signal is shifted in frequency due to a relative speed between the communication partners, or between the radar platform and reflecting objects, respectively. In the case of a communication link between two platforms moving with relative velocity v_{rel}, the Doppler frequency shift f_D at the receiver is

$$f_{D,comm} = \frac{v_{\mathrm{rel}}}{\lambda} = \frac{v_{\mathrm{rel}} f_c}{c_0} \tag{11}$$

with λ being the wavelength and f_c being the carrier frequency, respectively. In the case of the radar application, twice the Doppler shift occurs due to the two-way propagation [20]

$$f_{D,radar} = \frac{2v_{\mathrm{rel}}}{\lambda} = \frac{2v_{\mathrm{rel}} f_c}{c_0}. \tag{12}$$

Hence, the Doppler shift is more critical to the radar application; the applied waveform must be able to withstand the Doppler shift described by (12). It would be desirable, not only to design the radar application to be robust against Doppler shift, but also to allow an explicit estimation of the resulting Doppler shift in order to be able to determine the velocity difference of reflecting objects. However, with spread spectrum signals, this estimation is hardly possible. The only solution would be to calculate correlations similar to (5), but with copies of the original transmit signal shifted in frequency, which would require an extremely high computational effort that would hardly be feasible in practical real-time applications.

In order to make the system robust against Doppler shift, the frame duration $N_{\mathrm{sym}}LT$, over which the correlation is computed, must be short enough, so that the phase of the modulation symbols is not affected much by the Doppler shift during this time. In order to investigate the practical robustness of the studied concept, additional simulations are conducted with different Doppler shifts for an SIR of 0 dB. In Fig. 7, the available peak-to-side-lobe ratio, as a function of the Doppler shift and the spreading factor, is shown.

It can be seen that, higher spreading factors initially provide higher dynamic range, but the performance degrades more rapidly under the influence of Doppler, already at a few hundred Hz. Surprisingly, the PSL does not continuously decrease but starts increasing again at a certain Doppler shift, as can be seen for the $L = 255$ case. This behavior can be explained by the fact that integrating over a rotating phase results in a zero-order Bessel function. For example, with a carrier frequency of 24 GHz, a Doppler shift of $f_D = 1$ kHz corresponds to a relative velocity of $v_{\mathrm{rel}} = 6.25$ m/s (or, 22.5 km/h). As can be seen from Fig. 7, in scenarios with moving objects the PSL that can be achieved in radar measurements with spread spectrum signals is generally limited.

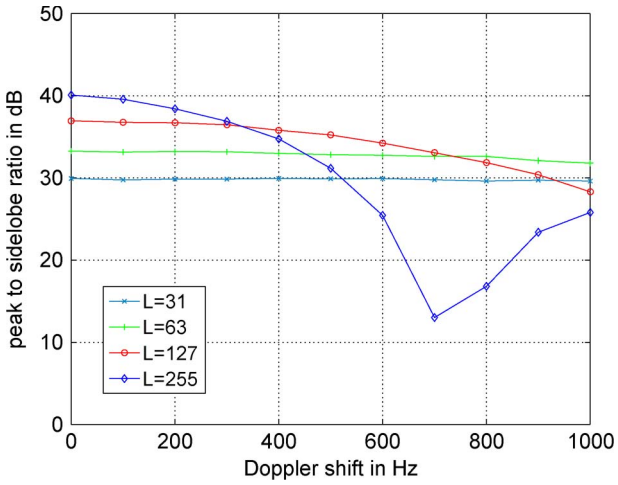

Fig. 7. ***Robustness against Doppler shift for different spreading factors.***

E. Conclusions on Single-Carrier Waveforms

It can be concluded that single-carrier communication signals, in combination with spread-spectrum techniques, are generally applicable for joint communications and radar applications. For the communications application, multiple-user operation is inherently possible, since the different users can be separated by user-specific codes. At the same time, the user data rate is reduced by the spreading factor. However, the dynamic range, in radar measurements, remains limited, as a result of the only quasi-perfect autocorrelation properties of the resulting transmit sequences. The best performance is obtained with long-code encoding and, either m-sequences or Kasami codes. In applications with moving objects, the integration time is limited due to the Doppler effect. With a system bandwidth on the order of 100 MHz, a dynamic range in the order of 40 dB can be achieved, even in the presence of interference and moderate Doppler shift. A major drawback for automotive applications is the fact that the estimation of the velocity of reflecting objects would require immense computational efforts.

IV. THE OFDM MULTI-CARRIER APPROACH

A. Classical Approaches to OFDM Signal Based Radar Sensing

OFDM signals have become a popular choice, in recent wireless communications standards, due to their robustness against fading and multipath propagation effects. Typical examples are the WLAN standards IEEE 802.11.a/g/n, their adaptation for car-to-car networks IEEE 802.11.p, as well as the current standardization process of the long-term evolution (LTE) standard, for high data rate mobile communications [21]. Also, in the radar community multicarrier signals recently have attracted interest in the context of frequency-agile waveforms, due to their ability to both flexibly occupying the available spectral resources and withstanding possible jammers [22]. In contrast to single-carrier waveforms, which are described by a single dimension along the time axis, multicarrier signals also incorporate diversity along the frequency dimension and, hence, can be interpreted as occupying a two-dimensional space in time and frequency. This fact offers manifold opportunities for applying sophisticated radar processing algorithms, which go far beyond the classical time domain correlation approach.

The first investigations on the suitability of multicarrier waveforms for radar applications were published in 2000 by Levanon [22], [23]. However, in his work the transmission of information by encoding and keying the phases of the individual carriers was not considered. The idea of introducing information into the multicarrier signal, by phase modulation of the subcarriers and realizing an efficient double use of the spectrum, appears only much later, in 2006 [5], [24]. In that context, now also the term OFDM, instead of *multicarrier*, has been explicitly used, assuming an OFDM signal as described by (2), including a cyclic prefix for each OFDM symbol. However, up to the present time, the possibility of explicitly exploiting the frequency dimension of the OFDM signal has still not been fully realized.

In the subsequent years, detailed system concepts for joint radar and communications applications have been presented. Garmatyuk *et al.* have developed a joint radar and communications OFDM system for applications according to the FCC ultra wideband (UWB) regulations [25], [26]. The system operates with a bandwidth of 500 MHz and covers only short ranges up to 5 m. The processing at the receiver is carried out by calculating the correlation function of the transmitted and received baseband signals. The provided results show a relatively low peak-to-side-lobe ratio, on the order of 15 dB. The first concept including Doppler processing of OFDM radar signals has been published by Tigrek *et al.* [27], [28]. The application in this case is an X-band surveillance radar network, with a signal bandwidth on the order of 1 MHz, and operating ranges on the order of 50 km; in this concept, the processing in the receiver is based on calculating correlation functions. In order to determine the Doppler, different correlation templates, corresponding to different Doppler shifts, are used. Besides the very high computational effort for the calculation of multiple correlation functions, this approach has the drawback of producing Doppler ambiguities at multiples of the subcarrier spacing for target distances above a certain limit, which depends on the choice of the OFDM system parameters. The authors identify the cyclic prefix and the interference between subsequent OFDM symbols as the reason for these ambiguities. In order to achieve an unambiguous radar image, also for large target distances, it is proposed to use a

special signal without cyclic prefix and a fixed phase constellation on the subcarriers, which would then, however, disable the communication functionality at the same time. Hence, it can be concluded that with the classic correlation-based processing approach, performance limits, regarding the peak-to-side-lobe ratio and ambiguities, remain. Moreover, all concepts that are based on the correlation processing approach do not explicitly consider the information content of the signal for optimizing the radar processing. The idea of developing a dedicated matched filter, that considers the multicarrier structure of the OFDM signal and compensates for the influence of the user data, was first described by Berger *et al.* in the context of passive radar applications [29], [30]. In this work, a solution for the estimation of the Doppler is also proposed, which evaluates the phase shift of the received signal versus time.

B. OFDM Radar Processing in the "Modulation Symbol" Domain

In the following, an advanced joint range and Doppler estimation algorithm for OFDM signals, developed by the authors, is considered, which allows a much simpler and intuitive description, because it directly operates on the transmitted and received modulation symbols, instead of the baseband signals. It is, therefore, referred to as processing in the "modulation symbol" domain. This approach fully exploits the two-dimensional signal structure of the OFDM signal and can be efficiently implemented at the same time. The general idea has been introduced in [31] for the range processing. In this approach, the user data is completely eliminated during the processing, which allows very high peak-to-side-lobes ratios, since the imperfect autocorrelation properties of the baseband signal will, then, not affect the estimation. A very similar concept, in the modulation symbol domain, can be applied for Doppler estimation in parallel [32].

In the following, we address, how both estimators can be combined into a two-dimensional estimator in the modulation symbol domain. In Fig. 8, a block scheme of the assumed OFDM system architecture is shown. The binary user data is divided into parallel streams, and mapped onto complex-valued PSK symbols resulting in the modulation symbol sequence $d_{Tx}(\mu, n)$. By a block-wise inverse fast Fourier transform, and a subsequent parallel-to-serial conversion, the time domain signal $x(t)$, composed of the orthogonal carrier waveforms f_n, is calculated. This signal is then converted to an analog signal and radiated at the carrier frequency, after being mixed with a local oscillator signal. In the receiver, the same steps are carried out in the inverse order. The received modulation symbols $d_{Rx}(\mu, n)$ are recovered from the received baseband signal $y(t)$ by a fast Fourier transform operation. While classical OFDM radar algorithms basically aim at exploiting the baseband signals $x(t)$ and $y(t)$, the following considerations will reveal an algorithm that allows for performing the radar measurement with the knowledge of the modulation symbols $d_{Tx}(\mu, n)$ and $d_{Rx}(\mu, n)$ only.

If an OFDM signal, as described by (2), is reflected at an object in the range R with a Doppler shift f_D due to a relative movement, the received signal can be described as

$$y(t) = \sum_{\mu=0}^{N_{\text{sym}}-1} \sum_{n=0}^{N_c-1} A(\mu, n) d_{Tx}(\mu N_c + n) \times \exp\left(j2\pi f_n \left(t - \frac{2R}{c_0}\right)\right) \exp(j2\pi f_D t) \times \text{rect}\left(\frac{t - \mu T_{\text{OFDM}} - \frac{2R}{c_0}}{T_{\text{OFDM}}}\right) \quad (13)$$

with $d_{Tx}(\mu, n)$ being the user data symbols which, in contrast to spread spectrum transmission, are not subject to any particular coding. In order to make the difference in the influence of range and Doppler more clearly visible, (13) can be rearranged into

$$y(t) = \sum_{\mu=0}^{N_{\text{sym}}-1} \exp(j2\pi f_D t) \sum_{n=0}^{N_c-1} A(\mu, n) \times \left\{ d_{Tx}(\mu N_c + n) \exp\left(-j2\pi f_n \frac{2R}{c_0}\right) \right\} \times \exp(j2\pi f_n t) \text{rect}\left(\frac{t - \mu T_{\text{OFDM}} - \frac{2R}{c_0}}{T_{\text{OFDM}}}\right). \quad (14)$$

The receiver recovers the individual modulation symbols related to one OFDM symbol by observing the received signal for only the elementary OFDM symbol duration $T < T_{\text{OFDM}}$. Provided that the guard interval duration T_G has been properly chosen, the receiver will still cut the observed samples from the same OFDM symbol and hence the time shift of the *rect*-function in (13) and (14) can be neglected. Regarding the individual modulation symbols it can be seen that, for a fixed OFDM symbol index μ, the Doppler frequency has no individual influence on the different modulation symbols within the same

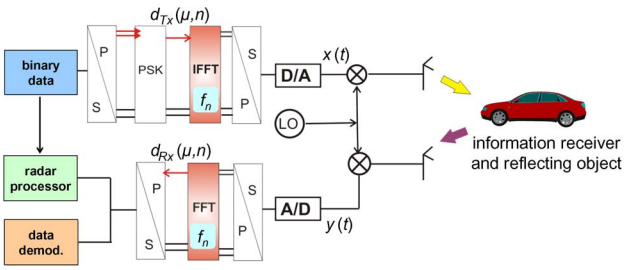

Fig. 8. ***Block scheme of the OFDM system architecture.***

OFDM symbol. Instead, the Doppler frequency causes an identical phase shift on every subcarrier, provided that the OFDM signal bandwidth is much smaller than the carrier frequency. On the other hand, for a fixed subcarrier index n, the Doppler effect introduces a linear phase shift between the consecutive modulation symbols on that subcarrier, corresponding to the phase change of the Doppler frequency during the total transmitted OFDM symbol duration $2\pi f_D T_{OFDM}$. Furthermore, the distance to the reflecting object does not have an influence on the phase shift between the subsequent modulation symbols on one subcarrier. The most important observation, however, is that, the range and the Doppler introduced by a reflecting object, have a completely orthogonal influence on the modulation symbols. While the range introduces a linear phase shift only along the frequency axis, the Doppler does the same, but only along the time axis. This orthogonality holds, provided that the observation duration is sufficiently short that the reflecting object remains within one range resolution cell. Hence, it must be possible to recover range and Doppler independently with a suitable processing algorithm.

Taking into account the subcarrier spacing from (3), and the relation between the relative velocity and the Doppler frequency from (12), the influence of a moving object on the received modulation symbols $d_{Rx}(n)$ can be quantified as

$$d_{Rx}(\mu N_c + n) = A(\mu, n) d_{Tx}(\mu N_c + n) \exp\left(-j2\pi n \Delta f \frac{2R}{c_0}\right) \times \exp\left(j2\pi \mu T_{OFDM} \frac{2v_{rel} f_c}{c_0}\right). \quad (15)$$

In order to arrive at a more descriptive representation, the modulation symbol frame is now regarded as a matrix, in which every column represents one OFDM symbol and every line represents one subcarrier as shown in (16) at the bottom of the page. This rearrangement can be applied to both the transmitted and the received modulation symbols, therefore, in (16) the subscripts have been omitted. Regarded in the same matrix representation, the received modulation symbols, after reflection at the moving object, result in

$$(\mathbf{D}_{Rx})_{\mu,n} = A(\mu, n)(\mathbf{D}_{Tx})_{\mu,n} \cdot (\vec{k}_R \otimes \vec{k}_D)_{\mu,n} \quad (17)$$

with $()_{\mu,n} \cdot ()_{\mu,n}$ indicating an element-wise multiplication of the matrices, $\otimes$ referring to a dyadic product, and

$$\vec{k}_R = \left(0 \quad \exp\left(-j2\pi\Delta f \frac{2R}{c_0}\right) \quad \cdots \quad \exp\left(-j2\pi(N_c - 1)\Delta f \frac{2R}{c_0}\right)\right) \quad (18)$$

and

$$\vec{k}_D = \left(0 \quad \exp\left(j2\pi T_{OFDM} \frac{2v_{rel} f_c}{c_0}\right) \quad \cdots \quad \exp\left(j2\pi(N_{sym} - 1) T_{OFDM} \frac{2v_{rel} f_c}{c_0}\right)\right) \quad (19)$$

describing independently the influence of range and the Doppler of the reflecting object on the received modulation symbols. From the description in (17), it is now clearly evident that these influences are orthogonal. In order to implement a processor for the estimation of range and relative velocity, in a first step the transmitted information has to be removed from the received information symbols by an element-wise complex division

$$(\mathbf{D}_{div})_{\mu,n} = \frac{(\mathbf{D}_{Rx})_{\mu,n}}{(\mathbf{D}_{Tx})_{\mu,n}} = A(\mu, n)(\vec{k}_R \otimes \vec{k}_D) \quad (20)$$

which results in the dyadic product of the two vectors carrying the range and the Doppler information. The only remaining task, that has to be accomplished, is to determine R from (18) and v_{rel} from (19). For that purpose, it is more convenient to return from the vector description back to an analytical representation, in which (18) and (19) change to

$$k_R(n) = \exp\left(-j2\pi n \Delta f \frac{2R}{c_0}\right) \quad (21)$$

$$\mathbf{D} = \begin{pmatrix} d(0) & d(N_c) & \cdots & d\big((N_{sym} - 1)N_c\big) \\ d(1) & d(N_c + 1) & \cdots & d\big((N_{sym} - 1)N_c + 1\big) \\ \vdots & \vdots & \ddots & \vdots \\ d(N_c - 1) & d(2N_c - 1) & \cdots & d(N_{sym} N_c - 1) \end{pmatrix} \quad (16)$$

and

$$k_D(\mu) = \exp\left(j2\pi\mu T_{\mathrm{OFDM}}\frac{2v_{\mathrm{rel}}f_c}{c_0}\right). \tag{22}$$

In (21), the range R translates into a linear phase shift between the modulation symbols along the frequency axis. The most convenient way to evaluate the range to the reflecting object, is to compute the inverse discrete Fourier transform of $k_R(n)$

$$\begin{aligned} r(k) &= \mathrm{IDFT}[k_R(n)] = \frac{1}{N_c}\sum_{n=0}^{N_c-1} k_R(n)\exp\left(j\frac{2\pi}{N_c}nk\right) \\ &= \frac{1}{N_c}\sum_{n=0}^{N_c-1}\exp\left(-j2\pi n\Delta f\frac{2R}{c_0}\right)\exp\left(j\frac{2\pi}{N_c}nk\right) \\ & \quad k = 0,\ldots,N_c-1. \end{aligned} \tag{23}$$

It can be seen that, the two exponential terms in (23) cancel each other and result in unity, under the condition

$$k = \left\lfloor\frac{2R\Delta f N_c}{c_0}\right\rfloor, \quad k = 0,\ldots,N_c-1 \tag{24}$$

which means that, at this index of k in the time response $r(k)$, a peak will occur. In a similar way, the determination of v_{rel} can be solved by applying a discrete Fourier transform to (22)

$$\begin{aligned} v(l) &= \mathrm{DFT}[k_D(\mu)] = \sum_{\mu=0}^{N_{\mathrm{sym}}-1} k_D(\mu)\exp\left(-j\frac{2\pi}{N_{\mathrm{sym}}}\mu l\right) \\ &= \sum_{\mu=0}^{N_{\mathrm{sym}}-1}\exp\left(j2\pi\mu T_{\mathrm{OFDM}}\frac{2v_{\mathrm{rel}}f_c}{c_0}\right) \\ &\quad\times\exp\left(-j\frac{2\pi}{N_{\mathrm{sym}}}\mu l\right),\ l = 0,\ldots,N_{\mathrm{sym}}-1 \end{aligned} \tag{25}$$

Cancellation of the exponential terms, and constructive superposition, results for the index:

$$l = \left\lfloor\frac{2v_{\mathrm{rel}}f_c T_{\mathrm{OFDM}}N_{\mathrm{sym}}}{c_0}\right\rfloor, \quad l = 0,\ldots,N_{\mathrm{sym}}-1. \tag{26}$$

The processing steps (23) and (25), are completely independent from the transmitted information. This guarantees a high dynamic range performance, since only the typical Fourier side-lobes can result. All processing steps are linear operations, which guarantees that the same approach will work for an unlimited number of reflecting objects with different distances and relative velocities.

The basis of a practical implementation of the algorithm is the received modulation symbol matrix $\mathbf{D_{Rx}}$. The complete processing consists of at least three steps. In the first step, the element-wise complex division according to (20) is performed for all matrix elements. As the next optional step, windowing functions can be applied to $\mathbf{D_{div}}$ along both matrix dimensions, in order to reduce the levels of the side-lobes introduced by the subsequent Fourier transforms. Then, in the second required step, the discrete Fourier transform of every row of $\mathbf{D_{div}}$ is computed. Finally, in the third step, the inverse discrete Fourier transform is calculated for every column of the matrix resulting from the previous step. The resulting matrix directly represents a two-dimensional radar image in range and Doppler. The complete algorithm is well-suited for practical applications, since it only requires the computation of discrete Fourier transforms, which is a standard procedure that can be efficiently implemented. Since the Fourier transforms include normalizations that can be more or less arbitrarily chosen, the resulting peak value in the radar image is not a measure for the processing gain. Instead, in each Fourier transform the signals add in a coherent deterministic process, resulting in a total power gain of N^2, whereas noise, as a stochastic quantity, only experiences a power gain of N. This results in a processing gain G_P from (23), equal to N_{sym} and, from (25), equal to N_c, respectively. Hence, the total processing gain G_P is

$$G_P = N_c N_{\mathrm{sym}}. \tag{27}$$

This is equivalent to the processing gain that would be achieved with a correlation processor under optimum conditions, which directly corresponds to the number of correlated samples. The modulation symbol-based processing algorithm offers the same performance regarding resolution and processing gain as a correlation processor. The processing gain of the modulation symbol-based processing approach has been verified with measurements that are published in [33]. The modulation symbol-based processing algorithm can also be interpreted as a maximum likelihood estimator. Considerations regarding this issue and detailed results for the estimation accuracy dependent on the SNR can be found in [34].

C. System Parameterization and Simulation Model

In order to find a suitable set of OFDM system parameters for practical vehicular applications, a parameter study for the 24 GHz ISM band has been conducted in [35], [36]. Most of the parameterization criteria are in fact identical, from both the communications and the radar perspective, since they are related to physical properties of

the channel. The limiting properties of the channel are, mainly, the Doppler spread and the maximum multipath delay. In general, these effects have a stronger influence on the radar application, since in this case always a factor of 2, due to the two-way propagation, is involved. Assuming a maximum relative velocity of $v_{\mathrm{rel,max}} = 200$ km/h in a typical traffic scenario (corresponding to $v_{\mathrm{rel,max}} = 55.6$ m/s) with (12) a maximum Doppler shift of the reflected signal of $f_{D,\mathrm{max}} = 8.9$ kHz must be expected. According to typical OFDM system design rules, the subcarrier spacing must be chosen to $\Delta f > 10 f_{D,\mathrm{max}}$ in order to ensure the orthogonality of the subcarriers [11]. The duration of the cyclic prefix must be chosen equivalent to the maximum expected delay difference between the different propagation paths. For the radar application it must be assumed, that there is direct coupling between the transmit and the receive antenna, hence the cyclic prefix duration must be chosen according to the roundtrip travel time between the system platform and the most distant target. Due to the high attenuation in radar measurements, and the power limitations of the 24 GHz ISM regulation of 20 dBm EIRP, a reasonable assumption is that the maximum detectable range is 200 m, which results in a minimum cyclic prefix duration of $T_G > 1.33\ \mu$s. For the communications application, this limit corresponds to a maximum delay difference, between the propagation paths, of 400 m. In Table 2, a complete set of OFDM system parameters, satisfying these conditions, is shown.

In addition to the physical limits of the channel, there are also restrictions that arise only for the radar operation and concern mainly possible ambiguities. With the symbol-based processing, the maximum measurement range corresponds to the distance that the signal travels during the elementary OFDM symbol duration T. However, the elementary symbol duration is typically much longer than the guard interval T_G, which means that by a suitable choice of the guard interval, there is no additional requirement for the choice of T that must be considered. The maximum absolute value of the Doppler shift f_D that can be measured, is limited by the time step between two consecutive OFDM symbols, which corresponds to T_{OFDM}. The maximum absolute Doppler shift that can be measured amounts to $1/(2T_{\mathrm{OFDM}})$. Hence, in order to cover a wide range of possible relative velocities v_{rel}, T_{OFDM} must be chosen as short as possible, which implies choosing the subcarrier spacing as large as possible. It is obvious that a joint optimum choice for both, range and Doppler measurement, does not exist. Instead, for the intended automotive application, a suitable tradeoff for the OFDM symbol duration must be found, that satisfies the requirements of typical road scenarios. As a conclusion, it can be remarked, that the parameter set in Table 2 fulfils all requirements, both from the communications and the radar perspective, and, hence, guarantees the simultaneous operability of both applications with high performance.

For the evaluation of the OFDM based approach, a complete simulation model, consisting of an OFDM transmitter, a point scatterer propagation model, and an OFDM receiver supporting both, correlation and modulation symbol-based processing, is also applied. In order to quantify the improvement that is achieved by the modulation symbol-based approach, compared to a standard correlation processor, first, range-only processing simulation results for one single reflecting object, are compared. In the simulations, the object is placed at a range of $R = 30$ m. Fig. 9 shows the normalized radar range profiles obtained by both processing techniques. The modulation symbol-based estimation was performed over $N_{\mathrm{sym}} = 256$ OFDM symbols including the application of a Hamming window.

Table 2 OFDM System Parameterization for the 24 GHz ISM Band

Symbol	Parameter	Value
f_c	Carrier frequency	24 GHz
N_c	Number of subcarriers	1024
Δf	Subcarrier spacing	90.909 kHz
T	Elementary OFDM symbol duration	11 µs
T_G	Cyclic prefix length	1.375 µs
T_{OFDM}	Total OFDM symbol duration	12.375 µs
B	Total signal bandwidth	93.1 MHz
ΔR	Radar range resolution	1.61 m
R_{max}	Unambiguous range	1650 m
$v_{\mathrm{rel,max}}$	Unambiguous velocity	± 253 m/s
N_{sym}	Number of evaluated symbols	256
Δv_{rel}	Velocity resolution	1.97 m/s
G_P	Processing gain	54.2 dB

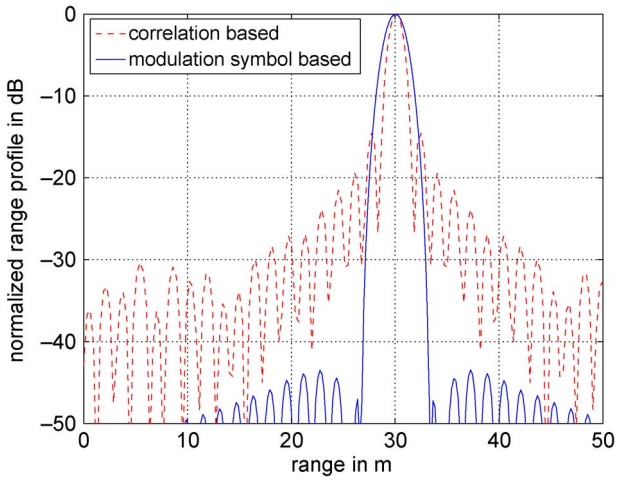

Fig. 9. *Radar image calculated from an OFDM signal, correlation processing versus modulation symbol based processing.*

It can be seen that the modulation symbol-based processing approach offers a drastically higher peak-to-side-lobe ratio. With the correlation processor, two undesired side-lobe effects show up. First, there are the typical Fourier first-order side-lobes at a level of around −15 dB. This might be surprising at first glance, since a correlation processor typically does not produce such side-lobes, however, these side-lobes appearing here are an inherent property of the OFDM signal and result from the rectangular pulse shaping in the OFDM transmitter. Second, there are additional side-lobes at a level of around −30 dB (e.g., for ranges between 0 and 10 m), which do not result from the Fourier transform, but from internal correlations in the transmit data. It must be assumed that when transmitting real user data, instead of random data, the level of these side-lobes may even increase. Even if the Fourier side-lobes resulting from the rectangular pulse shaping could by suppressed by a dedicated filter, there is no possibility to remove the side-lobes caused by the internal data correlations by a simple filter, since those are an inherent property of the transmit signal. On the other hand, with the modulation symbol-based processing approach, the peak-to-side-lobe ratio is only limited by the well-known Fourier side-lobes. Neither the side-lobes from the rectangular pulse shape, nor those from the correlations within the user data, appear. As a result of the Hamming window, the peak at the object position is widened.

The most important fact, however, is to show that the proposed modulation symbol-based algorithm is indeed able to estimate both range and Doppler, independently, for multiple reflecting objects. For that purpose a simulation is conducted with 3 point scatterers, two of them being placed at a range of $R = 30$ m and the third one at $R = 35$ m, while at the same time only the first scatterer has been assigned a relative velocity of $v_{\mathrm{rel}} = 5$ m/s and the 2nd and 3rd scatterers are moving with $v_{\mathrm{rel}} = 15$ m/s. In Fig. 10, the normalized radar image obtained with the modulation symbol-based processing approach for $N_{\mathrm{sym}} = 256$ is shown.

All three objects appear as single spots at their corresponding position of range and relative velocity in the radar image. As a consequence of the application of the Hamming window, the side-lobes are, again, attenuated well below −40 dB. The simulation result demonstrates that, multiple objects can be separated even if they are located in the same distance or have the same relative velocity. The estimation of range and Doppler is completely independent and orthogonal.

In order to get a better idea of the potential system performance, simulations with different noise levels and different numbers of evaluated OFDM symbols N_{sym} have been conducted. In particular, the $\mathrm{SNR}_{\mathrm{signal}}$ of the received baseband signal is varied between −40 dB and 40 dB. In the simulations, the resulting radar image signal-to-noise ratio $\mathrm{SNR}_{\mathrm{image}}$, which is the ratio between the peak caused by the object and the average noise level in the radar image, as well as the peak-to-side-lobe ratio (PSL), are evaluated for different values of N_{sym}, assuming one single point scatterer. In these simulations, a rectangular window is applied in order to avoid SNR loss, and the background noise level is evaluated without considering the side-lobes resulting from the rectangular window. In Fig. 11, the results for $\mathrm{SNR}_{\mathrm{image}}$ and *PSL* are presented as a function of $\mathrm{SNR}_{\mathrm{signal}}$. It can be seen that, in the double-logarithmic representation, both SNR_{image} and *PSL*, are improving linearly with SNR_{signal}. The difference between $\mathrm{SNR}_{\mathrm{image}}$ and PSL remains constant, at about 12 dB, when considering the same value of N_{sym}, which means that, in the worst case, the peaks in the background noise exceed

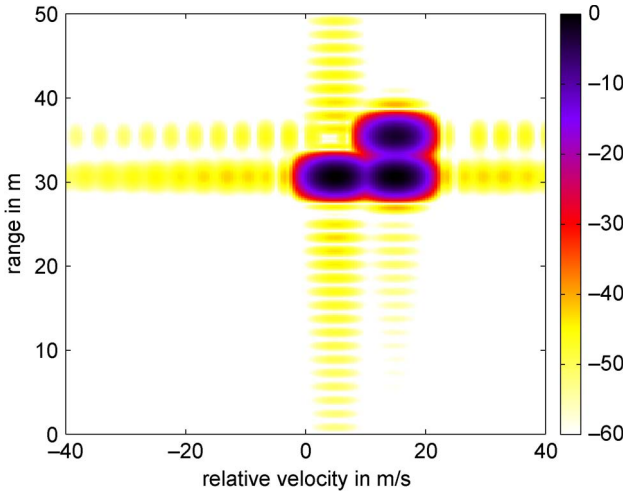

Fig. 10. *Normalized radar image calculated with modulation symbol based processing for 3 objects with $R = (30\ \mathrm{m}, 30\ \mathrm{m}, 35\ \mathrm{m})$ and $v_{\mathrm{rel}} = (5\ \mathrm{m/s}, 15\ \mathrm{m/s}, 15\ \mathrm{m/s})$, level in dB.*

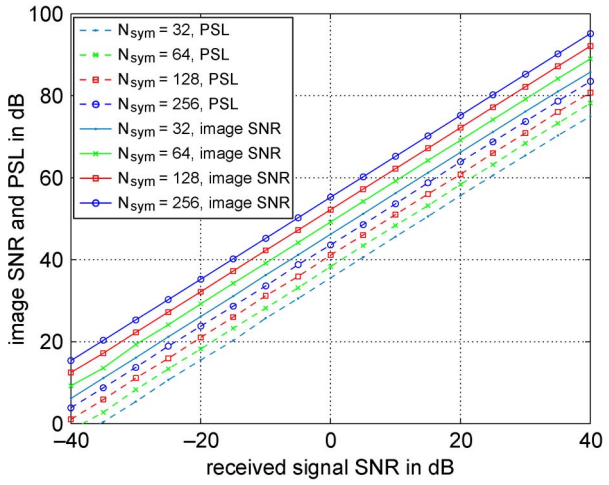

Fig. 11. *Radar image SNR and PSL dependent on the signal SNR for different numbers of evaluated OFDM symbols.*

the average background noise level by approximately 12 dB. By doubling the number of evaluated OFDM symbols N_{sym} the noise level decreases by 3 dB. The processing gain is very high and guarantees that, even for low $\mathrm{SNR}_{\mathrm{signal}}$, the background noise in the radar image is kept at a low level relative to the peak. The $\mathrm{SNR}_{\mathrm{image}}$ is 55.3 dB for an $\mathrm{SNR}_{\mathrm{signal}} = 0$ dB and $N_{\mathrm{sym}} = 256$, which corresponds to the processing gain theoretically expected from (27).

When comparing the results for the peak-to-side-lobe ratio of the OFDM system concept with the results obtained for the spread spectrum approach in Section III-C, it is evident that, with the OFDM approach, in combination with the modulation symbol-based processing, much higher peak-to-side-lobe ratios, of up to 80 dB, can be achieved. With the spread spectrum approach, the dynamic range tends to go into saturation at an $\mathrm{SNR}_{\mathrm{signal}}$ level of 0 dB, with dynamic ranges of around 40 dB. This effect does not occur with the OFDM-based approach, and the available peak-to-side-lobe ratio continuously grows with increasing SNR_{signal}. This behavior results from the fact that, in the modulation symbol-based processing approach, the transmitted user information is completely removed and cannot impact the result of the radar processing. Moreover, in the modulation symbol-based OFDM radar processing approach, the Doppler is inherently compensated, which means that the Doppler shift does not limit the integration time as for the spread spectrum approach.

It should be mentioned that, similar investigations have been conducted in order to study the influence of interference from other OFDM signals on the system performance. Exactly the same simulation model has been used, except for the fact that, instead of white noise, another OFDM signal with the same parameters, but different random user data, has been added to the received signal with different signal-to-interference ratios. It has turned out that, interference from another OFDM signal has exactly the same impact as the addition of white noise, i.e., only the background noise level rises, but no false targets appear. The results for SNR_{image} and PSL under the influence of OFDM interference are identical to the simulation results shown in Fig. 11. Hence, also the OFDM-based approach is very robust against interference, and the processing gain described by (27) applies against OFDM interference, as well.

D. System Demonstrator and Measurement Results

For the OFDM-based approach, a complete system demonstrator for operation in the 24 GHz ISM band has been set up, based on commercial measurement equipment. The main components of the setup are a Rohde & Schwarz (R&S) SMJ100A vector signal generator, a R&S SMR40 microwave signal generator, and a R&S FSQ26 signal analyzer. An additional medium power amplifier module, Hittite HMC498, is applied to increase the output power up to a level of 4.2 dBm. The signals are radiated and received with horn antennas providing a gain of approximately 22 dBi. The generation and processing of the signals is performed in MatLab using software components from the simulation model. The devices are controlled with the MatLab instrument control toolbox, which allows a quasi-realtime operation of the system. The implementation of the demontrator setup is described in detail in [33].

In order to test the performance of the OFDM-based concept in a real road scenario, the demonstrator setup is installed in a car for test drives. The horn antennas are mounted on a roof rack on top of the car. The remaining system components are placed in the trunk. The system parameters are set according to Table 2. Fig. 12 shows a photo of one particular motorway scenario that has been chosen, since it represents a worst-case scenario due to the strong reflection from the truck that is driving directly in front of the car with the RadCom system. All cars driving ahead are numbered in the photo.

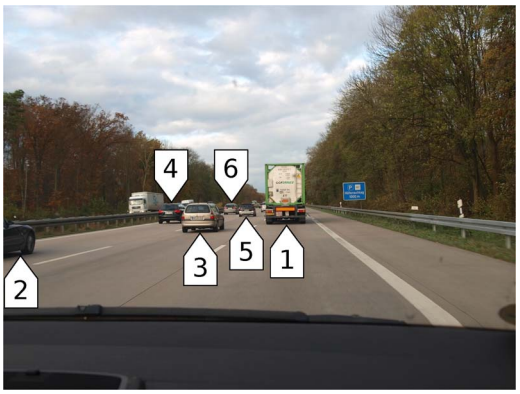

Fig. 12. *Photo of an investigated real road scenario.*

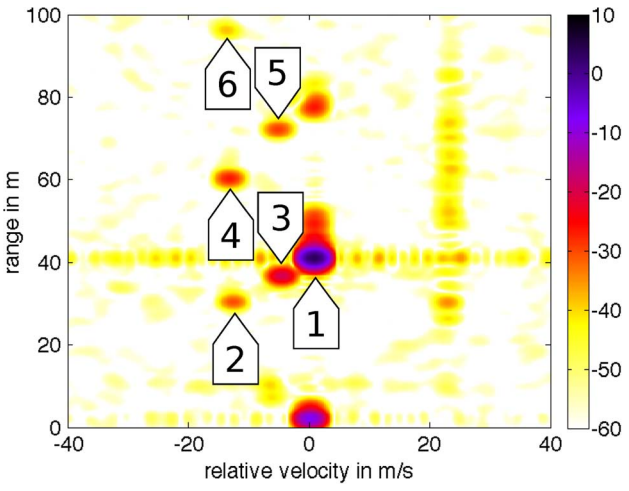

Fig. 13. *Radar image obtained in the scenario shown in Fig. 12, level in dB normalized to a radar cross section of 0 dBm² in a distance of 10 m.*

The radar image obtained from the reflected OFDM signal for this scenario is shown in Fig. 13, including numbers referring to the different cars in the corresponding photo. The image level has been normalized such that 0 dB corresponds to a radar cross section of $\sigma_{\mathrm{RCS}} = 0$ dBm^2 in a range of 10 m. The radar image shows a very high dynamic range and the reflecting objects appear very clearly. All cars can be identified in the radar image. The photo has been taken an instant earlier compared to the radar image, hence the distance of cars 2, 4, and 6 does not exactly coincide, when comparing the photo and radar measurement, due to their high relative velocity. For a close distance, a reflection appears with zero relative velocity, which is caused by the reflection from the chassis of the car. The strongest reflecting object is the truck (1) causing a reflection 23 dB higher, compared to the reflection from the second strongest object, which is car 3 on the middle lane. The reflection from the truck is 3.5 dB in the radar image, which translates into a radar cross section of $\sigma_{\mathrm{RCS}} = 25.5$ dBm^2, taking into account the distance. The radar cross section of the car on the middle lane is $\sigma_{\mathrm{RCS}} = 1.4$ dBm^2. In the radar image, the faster driving cars on the middle lane, (3) and (5), appear with a relative velocity of about -5 m/s (-18 km/h) and the cars on the left lane, (2), (4), and (6), at -12 m/s (-43.2 km/h). The side-lobes caused by the truck show a relative level of -38.5 dB along the Doppler axis, visible as a horizontal line in the range of 40 m, and are clearly weaker along the range axis with only -44.8 dB. The reduction along the range axis results from the transfer function of the lowpass filter at the input of the A/D-converter in the receiver, which provides an additional windowing effect. It is also interesting to see, that all reflections, from non-moving objects and the ground clutter, are visible as a vertical line with a relative velocity of 23 m/s (82.8 km/h), corresponding to the velocity of the test vehicle with the OFDM system platform. The background noise level is low. The radar image SNR has been determined to be $SNR_{\mathrm{image}} = 65.9$ dB (including the processing gain). The peak background noise level is -54.3 dB, with respect to the peak caused by the truck. This confirms the simulation results regarding the ratio between $\mathrm{SNR}_{\mathrm{image}}$ and PSL (cf. Fig. 11).

Hence, it can be concluded that the regarded processing technique in the modulation symbol domain provides an outstanding performance for practical applications in the 24 GHz ISM band. The available dynamic range is sufficient in order to detect all cars on the road, even if one single object causing a very strong reflection is present. The ability of determining the relative velocity, independently from the range, is an extremely useful feature, since it creates a second dimension that allows for distinguishing all moving objects from the clutter and the reflections from fixed objects.

E. Conclusions on Multicarrier Waveforms

With the application of multicarrier waveforms, and dedicated processing techniques that exploit the frequency dimension of these waveforms, the performance of the radar application can be drastically improved. The modulation symbol-based processing approach allows for the removal of the information and, hence, radar measurements can be performed, while transmitting arbitrary user data. At the same time, the dynamic range of the single-carrier spread spectrum approach is outperformed by many orders of magnitude, in particular, for high SNR levels, since the performance grows with increasing SNR without any saturation effects. Furthermore, it is possible to also estimate easily the relative velocity, independently from the range, for every reflecting object. A high gain is achieved in the radar processing that also is maintained in the presence of interference from other OFDM systems. Due to the inherent compensation of the Doppler shift in the modulation symbol-based processing algorithm, the integration time is not limited by the Doppler.

The operability of the concept, and the high dynamic range, have been verified by measurements with a system demonstrator in a real road scenario. For the communications application, special coding is not required. Therefore, for the single user, the entire bandwidth is available for data transmission, which allows very high data rates. However, for a multiple-user operation of the communications application, an additional multiple-access technique, e.g., time division multiple access (TDMA), is required.

V. MULTIPLE ANTENNA PROCESSING

The aim of waveform design is, not only to develop one common waveform for radar and communications applications, but also to include the possibility of effecting multiple antenna processing techniques for angular reflector location, at the receiver. The receiver structures of both

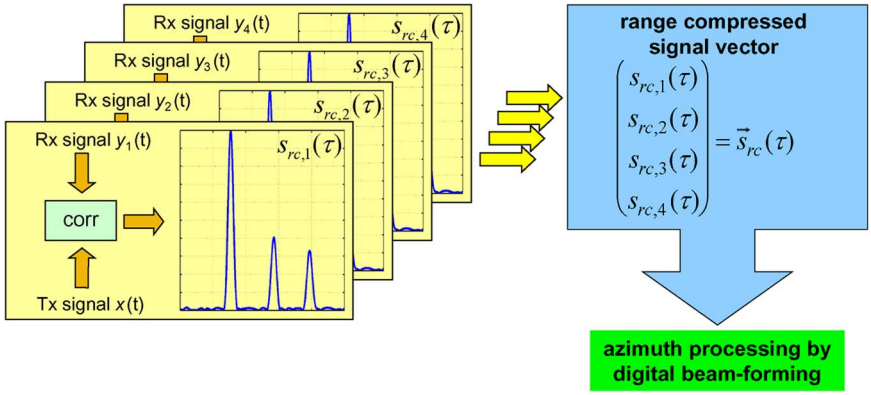

Fig. 14. *4 element DBF radar signal processing.*

digital beam-forming (DBF) radar systems and multiple input-multiple output (MIMO) communications systems provide one individual receiver for each receiving antenna, with each receiver consisting of baseband conversion and subsequent analog-to-digital conversion. Theoretically, multiple antenna processing techniques can be directly applied to the digitized baseband signals, however, this approach would require extremely high computational effort. For practical implementations, it is more convenient to effect the individual application processing first, e.g., in the case of the radar application, the range (and Doppler) compression. The multiple antenna techniques will, then, directly be applied to the output signals of these preprocessors. The combination of the signals for a linear array with four elements and the spread-spectrum-based approach, is illustrated in Fig. 14. As requirement for the applicability of multiple antenna processing techniques, these signals must contain amplitude and phase information. This is given for both, the spread spectrum range estimation described in (5) and the OFDM range and Doppler estimation, (23) and (25). In order to keep the description of the multiple antenna processing universal, in the following the expression $s_{rc}(\tau)$ will be used for the range compressed signal replacing, either $r_{yx}(\tau)$, from (5), or $r(k)$, from (23). In the case of the OFDM approach, the same algorithms can also be applied to the velocity estimation result without any restrictions.

For the radar application, multiple antenna processing is of particular interest, since it allows the estimation of the azimuth positions of scattering objects with the help of a linear antenna array. Therefore, the focus in the subsequent discussion will be on the direction of arrival estimation for the radar application. Nevertheless, the same approach can also be employed for the communications application, where it will allow improving the signal-to-noise ratio and also determination of the directions of distant transmitters.

More generally, assuming the receiver has an antenna array of P elements, the range-compressed pre-processor output signals $s_{rc}(\tau)$ can be arranged in a vector as

$$\vec{s}_{rc}(\tau) = \begin{pmatrix} s_{rc,1}(\tau) \\ s_{rc,2}(\tau) \\ \vdots \\ s_{rc,P}(\tau) \end{pmatrix}. \tag{28}$$

In the following, the application of two widely used multiple antenna processing approaches will be described and investigated. In order to limit the complexity of the equations, a horizontally oriented linear antenna array with constant element spacing d will be assumed. As a common basis, both approaches share the definition of a beam-steering vector, which is a vector that describes the samples of the complex wave front at the receiving antenna positions, provided that one single plane wave is impinging on the array from the azimuth angle ψ:

$$\vec{b}(\psi) = \begin{pmatrix} e^{j\sin(\psi)2\pi d/\lambda} \\ e^{j\sin(\psi)2\pi 2d/\lambda} \\ \vdots \\ e^{j\sin(\psi)2\pi Pd/\lambda} \end{pmatrix}. \tag{29}$$

First, the classical Fourier transform-based approach is considered, which consists of simply adding the elements of the range-compressed signal vector with additional phase shifts [37]. This corresponds to multiplying the range-compressed signal vector with the beam-steering vector. The radar image intensity I for any range τ and azimuth direction ψ is obtained as:

$$I(\tau,\psi) = \left|\vec{b}^{*}(\psi)\vec{s}_{rc}(\tau)\right|^{2}. \tag{30}$$

Including the structure of the beam-steering vector, this can be rewritten as:

$$I(\tau,\psi)=\left|\sum_{p=1}^{P} s_{rc}(\tau)\cdot e^{-jpu}\right|^2,\quad u=2\pi\cdot\frac{d}{\lambda}\cdot\sin(\psi) \quad (31)$$

which exactly corresponds to the structure of a discrete-time Fourier transform, but with sinusoidal distortion in the frequency domain.

Second, a multiple-antenna, high-resolution processing approach will be considered, that is more sophisticated. This approach is named MUSIC (Multiple Signal Classification), and has first been described in [38]. It operates on the eigen-structure of the correlation matrix of the range-compressed signal vector. The range-compressed signal vector for one specific range cell τ_0 containing $Q<P$ scatterers can be expressed as a linear combination of Q beam-steering vectors, each virtually oriented toward the direction of one single scatterer

$$\vec{s}_{rc}(\tau_0)=\left[\vec{b}(\psi_1)\quad\cdots\quad\vec{b}(\psi_Q)\right]\cdot\begin{pmatrix}a_1\\ \vdots\\ a_Q\end{pmatrix}+\vec{N} \quad (32)$$

with $a_1\ldots a_Q$ being the complex weights of the different scatterers and $\vec{N}$ being a vector of dimension P, representing the additive complex noise values at the receiving antennas. The matrix in (31), composed of the beam-steering vectors, will be denoted $\mathbf{B}$ in the following. Calculating the correlation matrix $\mathbf{R}_{ss}$ of the preprocessor output signal vector described by (32) results in

$$\mathbf{R}_{ss}=E\left\{\vec{s}_{rc}(\tau_0)\vec{s}_{rc}^{*\mathrm{T}}(\tau_0)\right\}=\mathbf{B}\mathbf{R}_{aa}\mathbf{B}^{\mathrm{H}}+\sigma_N^2\mathbf{I} \quad (33)$$

with $E\{\}$ denoting the expectancy operator, $\mathbf{R}_{aa}$ being the correlation matrix of the complex weights $a_1\ldots a_Q$, σ_N^2 being the noise power, and $\mathbf{I}$ being an identity matrix of dimension P.

Having a deeper look into this result, one can find that, in the case of zero noise power, it simplifies to $\mathbf{B}\mathbf{R}_{aa}\mathbf{B}^{\mathrm{H}}$. This matrix, of dimension P, has the rank P–Q, which means it has Q eigenvalues different from zero and P–Q eigenvalues identical to zero. If the signals are superimposed with noise, there will still remain a distinguishable difference in the eigenvalues of $\mathbf{R}_{ss}$ with Q high eigenvalues $\vec{e}_{s,i}$ caused by the influence of both signal and noise, and P–Q relatively small eigenvalues $\vec{e}_{n,i}$ caused by noise only. This property can be directly exploited in order to determine the number of scatterers in the specific range cell τ_0.

For the determination of the angular positions of the scatterers, a particular property of the sub-spaces, spanned by the eigenvectors related to the high and the relatively small eigenvalues, is taken into account. As can be inferred from (32), the vectors composing $\mathbf{B}$, and virtually pointing towards the scatterers, are linear combinations of the eigenvectors $\vec{e}_{s,i}$ related to the high eigenvalues of $\mathbf{R}_{ss}$. Hence, they must be orthogonal to the sub-space spanned by the eigenvectors $\vec{e}_{n,i}$ related to the small eigenvalues of $\mathbf{R}_{ss}$. With this property in mind, the following radar image pseudointensity is defined

$$I(\psi)=\frac{1}{\sum_{i=1}^{P-Q}\left|\vec{b}^{*}(\psi)\vec{e}_{n,i}\right|^2}. \quad (34)$$

In case the orthogonality condition is fulfilled, this expression will show a strong peak, since the denominator approaches zero. However, the result obtained when calculating this image pseudointensity is not directly related to the scattered power.

Next, an example simulation result is presented, that is obtained by applying both multiple antenna processing techniques in combination with the spread spectrum waveform. With the simulation model, two point scatterers in the same distance separated by 5° in azimuth have been assumed, with $P=4$ receiving antennas and an element distance of $d=\lambda/2$. First, the range compression has been performed according to (5), then both multiple antenna processing techniques described in (30) and (34) have been applied. The azimuth profile of the radar image in the range cell containing the scatterers is shown in Fig. 15.

In contrast to the classic Fourier transform-based approach, which yields a very broad main-lobe that does not allow for distinction between the two scatterers, the

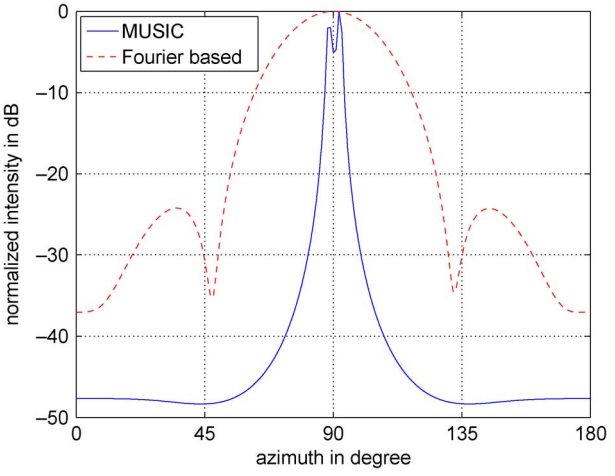

Fig. 15. ***Multiple antenna processing results for 2 scatterers separated by 5°, 4 antenna elements, spaced*** $d=\lambda/2$.

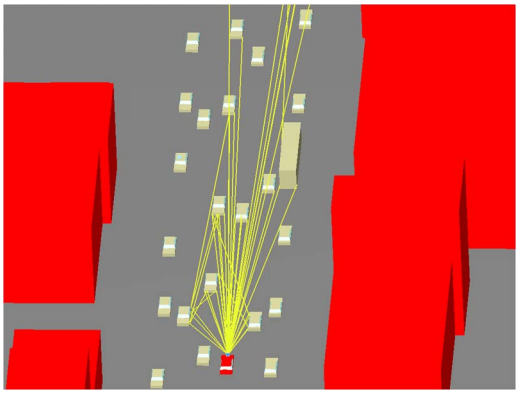

Fig. 16. *Investigated scenario in the propagation simulator.*

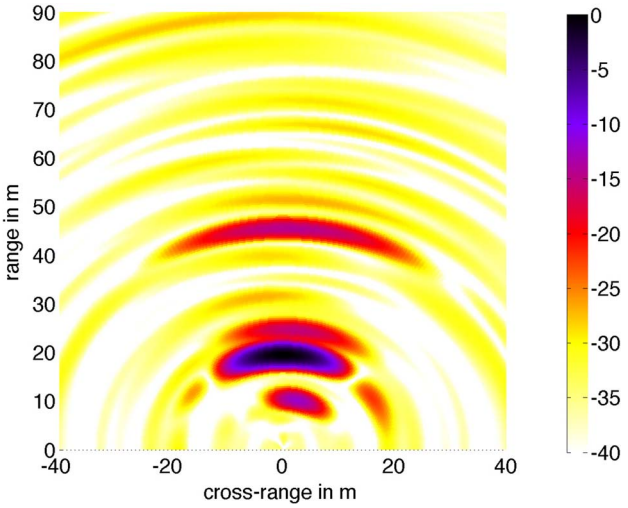

Fig. 17. *Radar image obtained with Fourier transform-based beamforming, normalized level in dB.*

MUSIC algorithm is able to clearly separate the two scatterers. Also, the Fourier-based approach shows considerably higher side-lobes (which had already been reduced in the processing by means of windowing), whereas the MUSIC algorithm offers a dynamic range of nearly 50 dB without any side-lobes.

In order to get an idea of the potential performance of the MUSIC algorithm in a more realistic scenario, the point scatterer model is replaced by a dedicated ray-tracing-based propagation simulator for road traffic environments. Besides the propagation simulation, this tool is also able to randomly create polygon object models of typical road environments, including the traffic flow based on a stochastic traffic model [39]. In the simulation tool, one car is equipped with the transmit and receive antennas of the RadCom system. The antennas are assigned cosine patterns with a half-power beamwidth of 30° in azimuth and 10° in elevation. In Fig. 16, the randomly created scenario, used for the investigations in this paper, is shown. The car being equipped with the radar system is colored in red. The yellow lines indicate the propagation paths (including paths with multiple reflections) from the transmit antenna to the receive antenna, that have been determined by the ray-tracing algorithm. Propagation paths that have an attenuation of more than 40 dB compared to the strongest path are not considered.

For every determined propagation path, time delay, attenuation, and phase shift are individually calculated, taking into account the dielectric material properties of the reflecting object and the antenna gain for the relevant direction under consideration, including the full polarization information. Then, all propagation paths are coherently superimposed, in order to obtain the instantaneous channel impulse response. The radar image obtained with the classical Fourier transform-based digital beamforming algorithm described in (30) for the investigated scenario is shown in Fig. 17.

Due to the low number of receiving antennas, and the half-wavelength spacing that is required in order to avoid ambiguities, the total aperture size is small, which allows only poor angular resolution. Only four reflecting objects can be detected in the radar image. The achievable position accuracy is rather low. Side-lobes caused by the strongest reflection are clearly visible. The radar image obtained for the same scenario with the MUSIC algorithm is shown in Fig. 18. With the same array configuration, a very high angular resolution is achieved. At least eight reflecting objects can be detected in the radar image, when considering all intensity values above −20 dB as a reflecting object. The nonlinearity of the MUSIC algorithm amplifies weaker reflections in the radar image and thus eases object detection. Obviously, all cars in Fig. 16, that only produce reflections below the −40 dB threshold, do not

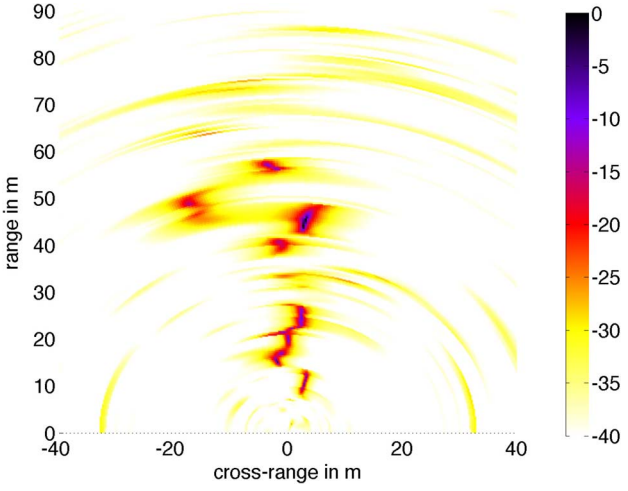

Fig. 18. *Radar image obtained with the MUSIC algorithm, normalized level in dB.*

appear in the radar image. Side-lobes, as in the Fourier-based processing, do not show up and the background noise is clearly reduced.

Hence, it has been verified that the proposed waveform design concepts are also suitable for the application of multiple antenna processing techniques. In the investigated system configuration, with only four receiving antennas, the MUSIC algorithm offers superior performance, compared to the classical Fourier-based approach. However, the MUSIC algorithm brings higher complexity and computational effort due to the required eigenvalue decomposition.

VI. RANGE PERFORMANCE CONSIDERATIONS

In the following, practical examples of the achievable ranges for radar and communication are calculated. The performance of both the communications and the radar application depends on a multiplicity of physical and system related parameters. For automotive radar, presently two frequencies are in operation, namely, 24 and 76 GHz. In the following as in the previous chapters a carrier frequency of 24 GHz is assumed. On the receive side, the noise figure is NF and the required signal-to-noise ratio is $\mathrm{SNR}_{\mathrm{signal}}$. At the receive antenna, the output $\mathrm{SNR}_{\mathrm{signal}}$ may vary widely; depending on the integration of the Radar signal and on the information coding, it may be even below 0 dB. The indices Tx and Rx stand for transmit and receive, respectively, and R for radar and C for communication. The antenna gain is G, the bandwidth B, and the power is P. As the number of parameters that influence both, radar and communication range, is rather high, certain assumptions will be made. For the calculation of the signal attenuation, line of sight propagation is assumed for both radar and communications. Typical system parameters and requirements are summarized in Table 3.

The assumed communication processing gain for the OFDM system of 10 dB, results from the application of redundancy coding, reducing, at the same time, the maximum possible data rate with QPSK modulation of 200 to 20 Mb/s. For DSSS, the communication processing gain corresponds to the spreading factor, reducing also the data rate from the chip rate of 100 Mb/s to 392 kb/s.

For the radar application the received signal power is calculated with the radar equation:

$$P_{Rx,R} = \frac{P_{Tx} G_{Tx} G_{Rx,R} \sigma_{RCS} \lambda^2}{(4\pi)^3 R_R^4}, \tag{35}$$

with σ_{RCS} being the radar cross section of the reflecting object, λ being the wavelength related to the carrier frequency, and R_R being the distance between the radar platform and the reflecting object. In the case of the

Table 3 Typical System Parameters of a Practical Implementation

Symbol	Value	Comment
General Parameters		
f_{Tx}	24 GHz	
$P_{\mathrm{Tx}}G_{\mathrm{Tx}}$	20 dBm	ISM limit 20 dBm EIRP
B	100 MHz	
P_N	-94 dBm	thermal noise kTB for 100 MHz
NF	6 dB	identical system noise Figure for radar and communications
L	255	spreading factor for spread spectrum/DSSS
Radar related parameters		
$\sigma_{\mathrm{RCS,min}}$	-10 dBm^2	worst case RCS
$G_{\mathrm{Rx,R}}$	20 dBi	HPBW 45° AZ, 9° EL
$\mathrm{SNR}_{\mathrm{image,R}}$	10 dB	
$G_{\mathrm{P,R,OFDM}}$	54.2 dB	$N_{\mathrm{sym}}N_c$, OFDM processing gain
$G_{\mathrm{P,R,DSSS}}$	45.1 dB	$N_{\mathrm{sym}}L$, DSSS processing gain
Communications related parameters		
$G_{\mathrm{Rx,C}}$	6 dBi	360° AZ, 30° EL
SNR_C	10 dB	
$G_{\mathrm{P,C,OFDM}}$	10 dB	
$G_{\mathrm{P,C,DSSS}}$	24.1 dB	equivalent to spreading factor $L = 255$

Table 4 Range Comparison for DSSS and OFDM Coded Radcom Systems

Modulation	Radar range	Comm. range	Data rate	$R_{max,C} / R_{max,R}$
DSSS	112 m	2512 m	392 kbit/s	22.4
OFDM	190 m	495 m	20 Mbit/s	2.61

communications application the received signal power results from the free space propagation law

$$P_{Rx,C} = \frac{P_{Tx} G_{Tx} G_{Rx,C} \lambda^2}{(4\pi)^2 R_C^2} \tag{36}$$

where R_C denotes the distance between transmitter and receiver. For the calculation of the SNR the thermal noise power and the receiver noise figure NF has to be taken into account

$$\mathrm{SNR} = \frac{P_{Rx}}{P_N NF} = \frac{P_{Rx}}{kBT_{\mathrm{abs}} NF} \tag{37}$$

with k being the Boltzmann constant and T_{abs} being the absolute temperature.

In the performance calculation it must be considered that a processing gain G_P is available for communications as well as for radar operation. The maximum range for the radar operation follows from (35) and (37) and results in

$$R_{\max,R} = \sqrt[4]{\frac{P_{Tx} G_{Tx} G_{Rx,R} G_{P,R} \sigma \lambda^2}{P_N \cdot NF_R \cdot \mathrm{SNR}_{\mathrm{image},R} \cdot (4\pi)^3}} \tag{38}$$

and the maximum range for communication is obtained from (36) and (37):

$$R_{\max,C} = \sqrt[2]{\frac{P_{Tx} G_{Tx} G_{Rx,C} G_{P,C} \lambda^2}{P_N \cdot NF_C \cdot \mathrm{SNR}_C \cdot (4\pi)^2}}. \tag{39}$$

From the above equations, the ranges compare as follows:

$$\frac{R_{\max,C}}{R_{\max,R}} = \sqrt{\frac{G_{Rx,C} G_{P,C} \lambda}{NF_C \mathrm{SNR}_C P_N}} \sqrt[4]{\frac{P_{Tx} G_{Tx} NF_R \mathrm{SNR}_{\mathrm{image},R} 4\pi \cdot P_N}{G_{Rx,R} G_{P,R} \sigma}} \tag{40}$$

The evaluation of the above (38)–(40) renders the results summarized in Table 4.

As can be seen in Table 4, both concepts render radar and communications performance that is suitable for practical applications. The higher radar range is achieved with OFDM modulation, due to the correspondingly higher radar processing gain. For automotive applications, the radar range should be 250 m in the ideal case. This would require some changes in the example parameters. Parameters that may be varied for special applications are the bandwidth B, the integration duration (processing gain), the hardware system parameters G_{Tx}, G_{Rx}, P_{Tx} or the noise figure NF. DSSS has a reduced radar range, however, it exhibits also a higher communication range. Nevertheless, the OFDM concept seems to provide the better trade-off among all performance criteria, taking also into account the considerably higher user data rate.

VII. CONCLUSION

Presently, the idea of mobile-to-mobile communications is based on the availability of specifically assigned spectrum, for example, at 5.9 GHz. But, as is well known, much wider spectra are available for automotive radar at 24 GHz and 76 GHz. It has been shown in this paper, that these radar spectra can be coded with information without any negative influence on the radar performance. On the other hand, with the presented concepts, car-to-car communication systems in the 5.9 GHz band can be equipped with additional radar features.

Two different waveform design concepts have been studied that allow for simultaneous wireless communications and radar operation, namely, OFDM and DSSS. The operability and the performance of both approaches have been comprehensively evaluated. The implementation, with multicarrier signals (OFDM), has been shown to offer many advantages regarding the performance of the radar application, in particular, very high dynamic range, independence from the transmitted user data, the possibility of estimating the relative velocity, and efficient implementation based on fast Fourier transforms. On the other hand, the spread spectrum approach (DSSS) facilitates the separation of multiple users for the communications application. The operability of the OFDM approach in practical road scenarios has been verified with a dedicated system demonstrator.

It has also been shown, that receivers with multiple antennas and processing techniques for direction of arrival estimation are well supported by these waveforms. For angular focusing, in particular, besides the classical

Fourier-based approach, the MUSIC algorithm, an approach that provides high angular resolution, with only four receiving antennas, has been found. It can be concluded that the discussed waveform design and signal processing concepts offer interesting perspectives for the realization of future intelligent sensor devices, that jointly perform spectrally-efficient radar sensing and communications, with one common signal, and with a cost-effective implementation, with one common hardware system. ■

REFERENCES

[1] M. I. Skolnik, *Radar Handbook*, 3rd. New York: McGraw-Hill, 2008.

[2] G. N. Saddik, R. S. Singh, and E. R. Brown, "Ultra-wideband multifunctional communications/radar system," *IEEE Trans. Microw. Theory Techn.*, vol. 55, no. 7, pp. 1431–1437, Jul. 2007.

[3] S. D. Blunt, P. Yatham, and J. Stiles, "Intrapulse radar-embedded communications," *IEEE Trans. Aerosp. Electron. Syst.*, vol. 46, no. 3, pp. 1185–1200, Jul. 2010.

[4] K. Mizui, M. Uchida, and M. Nakagawa, "Vehicle-to-vehicle communication and ranging system using spread spectrum technique," in *Proc. IEEE Veh. Technol. Conf.*, May 1993, pp. 335–338.

[5] B. J. Donnet and I. D. Longstaff, "Combining MIMO radar with OFDM communications," in *Proc. 3rd European Radar Conf. 2006*, Sep. 2006, pp. 37–40.

[6] M. Younis and W. Wiesbeck, "SAR with digital beamforming on receive only," in *Proc. IEEE Int. Geosci. Remote Sensing Symp.*, Hamburg, Germany, 1999, pp. 1773–1775.

[7] I. G. Cumming and F. H. Wong, *Digital Processing of Synthetic Aperture Radar Data: Algorithms and Implementation*. Norwood, MA: Artech House, 2005.

[8] D. Saunders, S. Bingham, G. Menon, D. Crockett, J. Tor, R. Mende, M. Behrens, N. Jain, A. Alexanian, and Rajanish, "A single-chip 24 GHz SiGe BiCMOS transceiver for FMCW automotive radars," in *Proc. IEEE Radio Frequency Integr. Circuits Symp.*, Jun. 2009, pp. 459–462.

[9] F. E. Nathanson, *Radar Design Principles*, 2nd ed. New York: McGraw-Hill, 1991.

[10] N. Levanon, "Multifrequency complementary phase-coded radar signal," *IEE Proc. Radar, Sonar and Navigation*, vol. 147, no. 6, pp. 276–284, Dec. 2000.

[11] M. Engels, *Wireless OFDM Systems: How to Make them Work?* Boston, MA: Kluwer Academic, 2002.

[12] K. Mizutani and R. Kohno, "Inter-vehicle spread spectrum communication and ranging system with concatenated EOE sequence," *IEEE Trans. Intell. Transport. Syst.*, vol. 2, no. 4, pp. 180–191, Dec. 2001.

[13] V. P. Ipatov, *Spread Spectrum and CDMA: Principles and Applications*. New York: Wiley, 2005.

[14] C. Sturm and W. Wiesbeck, "Waveform design for joint digital beamforming radar and MIMO communications operability," in *Principles of Waveform Diversity and Design*. Raleigh, NC: SciTech, 2010.

[15] L. R. Welch, "Lower bounds on the maximum cross correlation of signals," *IEEE Trans. Inf. Theory*, no. 20, pp. 397–399, 1974.

[16] S. Golomb, *Shift Register Sequences*. New York: Holden Day, (Revised edition: 1982 Aegean Park Press, Laguna Hills, CA), 1967.

[17] T. Kasami, "Weight Distribution Formula for Some Class of Cyclic Codes," Coordinated Sci. Lab., Univ. Illinois, Urbana-Champaign, Tech. Rep. R-285 (AD 632574), 1966.

[18] R. Gold, "Optimal binary sequences for spread spectrum multiplexing," *IEEE Trans. Inf. Theory*, pp. 619–621, Oct. 1967.

[19] F. C. M. Lau and C. K. Tse, *Chaos-Based Digital Communication Systems*. Berlin, Germany: Springer, 2003.

[20] B. R. Mahafza, *Radar Signal Analysis and Processing Using MatLab*. Boca Raton, FL: Chapman and Hall/CRC, 2009.

[21] T. S. Rappaport, A. Annamalai, R. M. Buehrer, and W. H. Tranter, "Wireless communications: Past events and a future perspective," *IEEE Commun. Mag.*, vol. 40, no. 5, pp. 148–161, May 2002.

[22] N. Levanon, "Multifrequency radar signals," in *Proc. IEEE Int. Radar Conf.*, May 2000, pp. 683–688.

[23] N. Levanon, "Multifrequency Signal Structure for Radar Systems," U.S. Patent 6 392 588, May 21, 2002.

[24] G. Lellouch, P. Tran, R. Pribic, and P. van Genderen, "OFDM waveforms for frequency agility and opportunities for Doppler processing in radar," in *Proc. IEEE 2008 Radar Conf. (RADAR 2008)*, May 26–30, 2008, pp. 1–6.

[25] A. Garmatyuk, J. Schuerger, Y. T. Morton, K. Binns, M. Durbin, and J. Kimani, "Feasibility study of a multi-carrier dual-use imaging radar and communication system," in *Proc. 37th European Microw. Conf.*, Munich, Germany, Oct. 2007, pp. 1473–1476.

[26] D. Garmatyuk, J. Schuerger, and K. Kauffman, "Multifunctional software-defined radar sensor and data communication system," *IEEE Sensors J.*, vol. 11, no. 1, pp. 99–106, Jan. 2011.

[27] R. F. Tigrek, W. de Heij, and P. van Genderen, "Multi-carrier radar waveform schemes for range and Doppler processing," in *Proc. IEEE 2009 Radar Conf.*, May 4–8, 2009, pp. 1–5.

[28] R. F. Tigrek, W. de Heij, and P. van Genderen, "A Method for Measuring the Radial Velocity of a Target With a Doppler Radar," European Patent Filing No. EP 08162331.6.

[29] C. R. Berger, S. Zhou, P. Willett, B. Demissie, and J. Heckenbach, "Compressed sensing for OFDM/MIMO radar," in *Proc. 42nd Asilomar Conf. Signals, Syst., Comput.*, Oct. 26–29, 2008, pp. 213–217.

[30] C. R. Berger, B. Demissie, J. Heckenbach, P. Willett, and S. Zhou, "Signal processing for passive radar using OFDM waveforms," *IEEE J. Sel. Topics Signal Process.*, vol. 4, no. 1, pp. 226–238, Feb. 2010.

[31] C. Sturm, E. Pancera, T. Zwick, and W. Wiesbeck, "A novel approach to OFDM radar processing," in *Proc. IEEE 2009 Radar Conf. (RadarCon09)*, Pasadena, CA, May 2009, [CD-ROM].

[32] C. Sturm, M. Braun, T. Zwick, and W. Wiesbeck, "A multiple target Doppler estimation algorithm for OFDM based intelligent radar systems," in *Proc. European Radar Conf. 2010*, Paris, France, Sep. 2010.

[33] C. Sturm, M. Braun, T. Zwick, and W. Wiesbeck, "Performance verification of symbol-based OFDM radar processing," in *Proc. IEEE 2010 Radar Conf.*, Washington, DC, May 2010.

[34] M. Braun, C. Sturm, and F. K. Jondral, "Maximum likelihood speed and distance estimation for OFDM radar," in *Proc. IEEE 2010 Radar Conf.*, Washington, DC, May 2010.

[35] C. Sturm, T. Zwick, and W. Wiesbeck, "An OFDM system concept for joint radar and communications operations," in *Proc. IEEE 69th Veh. Technol. Conf.*, Barcelona, Spain, Apr. 2009, [CD-ROM].

[36] M. Braun, C. Sturm, A. Niethammer, and F. K. Jondral, "Parametrization of joint OFDM-based radar and communication systems for vehicular applications," in *Proc. 20th IEEE Symp. Personal Indoor and Mobile Radio Commun. PIMRC 2009*, Tokyo, Japan, Sep. 2009.

[37] L. C. Godara, "Application of antenna arrays to mobile communication, Part II: Beam-forming and direction-of-arrival considerations," *Proc. IEEE*, vol. 85, pp. 1195–1245, Aug. 1997.

[38] R. O. Schmidt, "Multiple emitter location and signal parameter estimation," *IEEE Trans. Antennas Propagat.*, vol. 34, pp. 276–280, Mar. 1986.

[39] J. Maurer, T. Fügen, S. Knörzer, and W. Wiesbeck, "A ray-optical approach to model the inter-vehicle transmission channel," *Frequenz, J. RF-Eng. Telecommun.*, vol. 60, no. 5–6, pp. 95–98, May/Jun. 2006.

ABOUT THE AUTHORS

Christian Sturm (Student Member, IEEE) received the Dipl.-Ing. degree (M.Sc. equivalent) in electrical engineering and information technologies from Universität Karlsruhe (TH), Germany, in 2005.

In February 2005, he joined the Institut für Hochfrequenztechnik und Elektronik (IHE) at the Karlsruhe Institute of Technology as Research Associate. He serves as a Lecturer for the Carl-Cranz-Series for Scientific Education and for the European School of Antennas (ESoA). His research areas include concepts for joint implementations of radar and wireless communications, OFDM-based radar, multiple antenna systems, ultrawideband components and systems, and signal processing.

Mr. Sturm is a management committee member of the European COST action ic0803 RFCSET (RF/Microwave Communication Subsystems for Emerging Wireless Technologies). In 2010, he received the European Microwave Week Radar Award for the paper that best advances the state-of-the-art in radar.

Werner Wiesbeck (Fellow, IEEE) received the Dipl.-Ing. (M.S.) and the Dr.-Ing. (Ph.D.) degrees in electrical engineering from the Technical University Munich, Germany, in 1969 and 1972, respectively.

From 1972 to 1983, he was with AEG-Telefunken in various positions including that of Head of R&D of the Microwave Division in Flensburg and Marketing Director of Receiver and Direction Finder Division, Ulm. During this period, he had product responsibility for millimeter-wave radars, receivers, direction finders, and electronic warfare systems. From 1983 to 2007, he was the Director of the Institut für Höchstfrequenztechnik und Elektronik (IHE) at the University of Karlsruhe (TH) and he is now Distinguished Scientist at the Karlsruhe Institute of Technology (KIT). His research topics include antennas, wave propagation, radar, remote sensing, wireless communication, and ultrawideband technologies. In 1989 and 1994, respectively, he spent a six-month sabbatical at the Jet Propulsion Laboratory, Pasadena, CA.

Dr. Wiesbeck is a member of the IEEE GRS-S AdCom (1992–2000), Chairman of the GRS-S Awards Committee (1994–1998, 2002–), Executive Vice President IEEE GRS-S (1998–1999), President IEEE GRS-S (2000–2001), Associate Editor IEEE-AP Transactions (1996–1999), past Treasurer of the IEEE German Section (1987–1996, 2003–2007). He has been General Chairman of the 1988 Heinrich Hertz Centennial Symposium, the 1993 Conference on Microwaves and Optics (MIOP '93), the Technical Chairman of International mm-Wave and Infrared Conference 2004, Chairman of the German Microwave Conference GeMIC 2006, and he has been a member of the scientific committees and TPCs of many conferences. For the Carl Cranz Series for Scientific Education, he serves as a permanent lecturer for Radar systems engineering, wave propagation and mobile communication network planning. He is a member of an Advisory Committee of the EU—Joint Research Centre (Ispra/Italy), and he is an Advisor to the German Research Council (DFG), to the Federal German Ministry for Research (BMBF) and to industry in Germany. He is the recipient of a number of awards, lately the IEEE Millennium Award, the IEEE GRS Distinguished Achievement Award, the Honorary Doctorate (Dr. h.c.) from the University Budapest/Hungary, the Honorary Doctorate (Dr.-Ing. E.h.) from the University Duisburg/Germany and the IEEE Electromagnetics Award 2008. He is a Fellow of IEEE, an Honorary Life Member of IEEE GRS-S, a Member of the IEEE Fellow Committee, a Member of the Heidelberger Academy of Sciences and Humanities, and a Member of the German Academy of Engineering and Technology (ACATECH).